SYNTHESIS AND APPLICATIONS OF NANOPARTICLES IN BIOSENSING SYSTEMS

Sergio Marín Mancebo

Nanobioelectronics and Biosensors Group, Catalan Institute of Nanotecnology
Bellaterra, Barcelona, Spain

&

Grup de Sensors i Biosensors, Department de Química, Universitat Autònoma de Barcelona.

April 2009

Supporting information

DETECTION OF CADMIUM SULPHIDE NANOPARTICLES BY USING SCREEN-PRINTED ELECTRODES AND A HAND HELD DEVICE

Arben Merkoçi[1*], Luiz Humberto Marcolino-Junior[2], Sergio Marín[1]

Orlando Fatibello-Filho[2], Salvador Alegret[1]

[1]Grup de Sensors & Biosensors, Departament de Química, Universitat Autònoma de Barcelona, 08193 Bellaterra, Catalonia, Spain

[2] Laboratório de Bioanalítica, Departamento de Química, Universidade Federal de São Carlos, Rod. Washington Luiz, km 235, C. P. 676, 13560-970-São Carlos/SP- Brazil

*** Corresponding author**

[*] Corresponding author

E-mail: arben.merkoci@uab.cat; phone: +34-935811976; fax: +34-93581 2379

Contents

Figure 1S. SW Anodic stripping voltammograms for Cd^{2+} detection with the corresponding calibration curve (inset) performed with a screen-printed electrode using a volume of 20 μL under the electrode surface in 0.1 mol L^{-1} HCl. Increasing concentration of Cd^{2+}: (a) 10, (b) 100, (c) 250, (d) 500 and (e) 1000 ppb. Square-wave voltammetric scan with frequency of 25 Hz, step potential 10 mV and amplitude of 30 mV. Deposition potential of -1.1 V during 120 s

Figure 2S. Linear sweep voltammograms using the SPE (**A**) and a plot of the peak current *vs.* the square root of potential sweep rate (**B**). Scan speed of 10 to 500 mV s^{-1}. Conditions: supporting electrolyte 0.1 mol L^{-1} phosphate buffer (pH 7.0); accumulation time: 60 s; electrochemical reduction time: 120 s; reduction potential: -1.1 V; start potential: -1.1 V.

Figure 3S. HRTEM image of CdS QDs prepared as described in the text.

Figure 1S

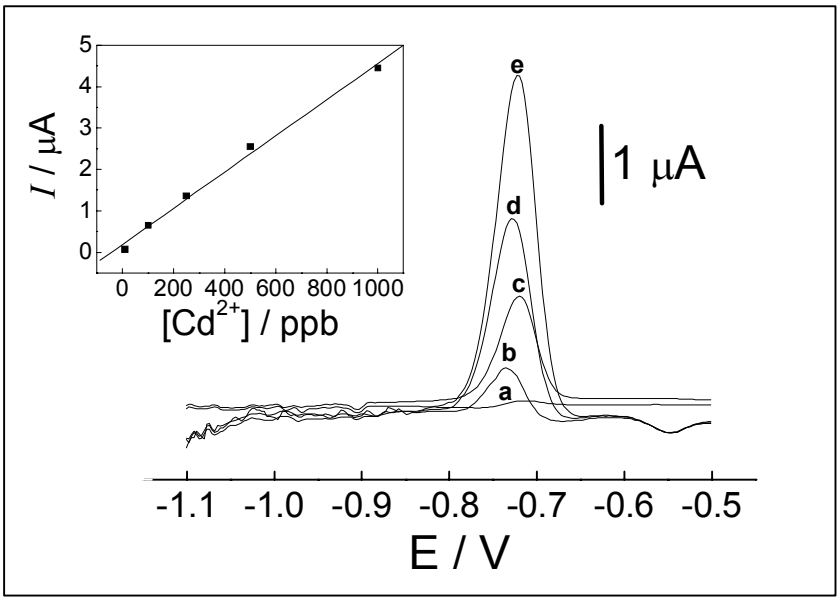
I / μA
0
1
2
3
4
5
0 200 400 600 800 1000
[Cd2+] / ppb
e
d
c
b
a
1 μA
-1.1 -1.0 -0.9 -0.8 -0.7 -0.6 -0.5
E / V

Figure 2S

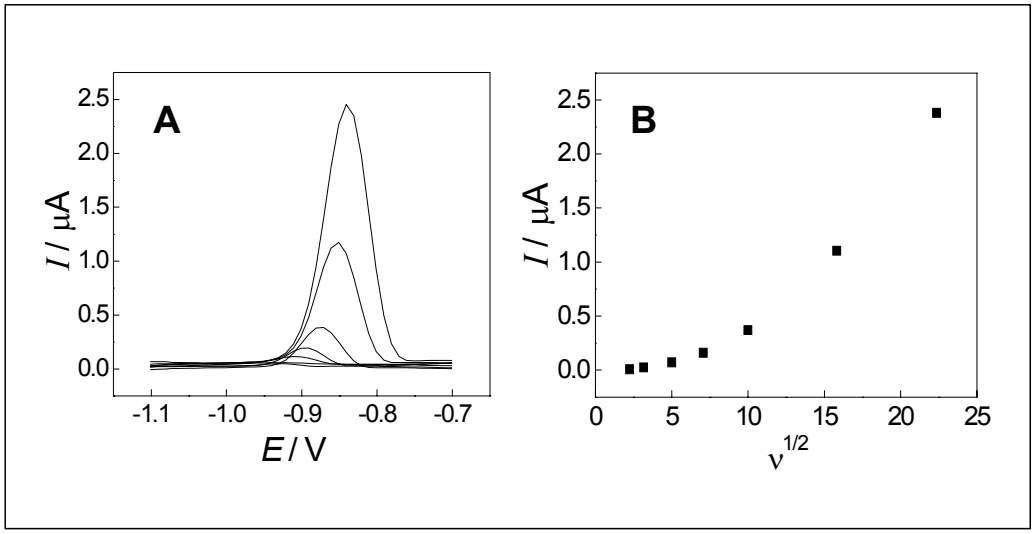

Figure 3S

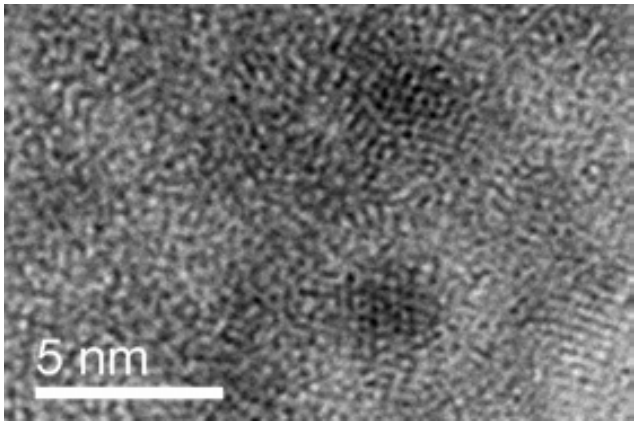

Silver, gold and the corresponding core shell nanoparticles: synthesis and characterization

Douglas F., Yañez R., Ros J., **Marín S**., de la Escosura-Muñiz A., Alegret S., Merkoçi A.

Journal of Nanoparticle Research

10, 9374-9384 (2008)

J Nanopart Res
DOI 10.1007/s11051-008-9374-3

RESEARCH PAPER

Silver, gold and the corresponding core shell nanoparticles: synthesis and characterization

Fraser Douglas · Ramon Yañez · Josep Ros · Sergio Marín · Alfredo de la Escosura-Muñiz · Salvador Alegret · Arben Merkoçi

Received: 1 October 2007 / Accepted: 6 February 2008

Abstract Simple strategies for producing silver and gold nanoparticles (AgNP and AuNP) along with the corresponding core shell nanoparticles (Au–Ag and Ag–Au) by reduction of the metal salts $AgBF_4$ and $HAuCl_4$ by $NaBH_4$ in water will be presented. The morphologies of the obtained nanoparticles are determined by the order of addition of reactants. The obtained NPs, with sizes in the range 3–40 nm, are characterized by transmission electronic microscopy (TEM) and UV–Vis absorption spectroscopy, so as to evaluate their qualities. Moreover, a direct electrochemical detection protocol based on a cyclic voltammetry in water solution that involves the use of glassy carbon electrode is also applied to characterize the prepared NPs. The developed NPs and the related electroanalytical method seem to be with interest for future sensing and biosensing applications including DNA sensors and immunosensors.

Keywords Gold nanoparticles · Silver nanoparticles · Au–Ag nanoparticles · Ag–Au nanoparticles · Cyclic voltammetry · Colloids

The author Fraser Douglas is on leave from: Chemistry Department, University of Glasgow, Glasgow G12 8QQ, UK.

Electronic supplementary material The online version of this article (doi:10.1007/s11051-008-9374-3) contains supplementary material, which is available to authorized users.

F. Douglas · R. Yañez · J. Ros
Unitat de Química Inorgànica, Departament de Química, Universitat Autònoma de Barcelona, 08193 Bellaterra, Catalonia, Spain

S. Marín · A. de la Escosura-Muñiz · A. Merkoçi
Nanobioelectronics & Biosensors Group, Institut Català de Nanotecnologia, Bellaterra, Catalonia, Spain

S. Marín · S. Alegret · A. Merkoçi (✉)
Group of Sensors & Biosensors, Departament de Química, Universitat Autònoma de Barcelona, 08193 Bellaterra, Catalonia, Spain
e-mail: arben.merkoci.icn@uab.es

Introduction

There is currently immense interest surrounding the synthesis and characterisation of mono- and bimetallic nanoparticles. This field presents a broad scope of research, as nanoparticles (NPs) can exhibit unusual chemical, physical and electrical properties that are not apparent in bulk materials (Schmid 1992; Mulvaney 1996), as well as possessing size-dependent properties and the potential for constructing nano- and micro assemblies (Ozin 1992). The field of bimetallic nanoparticle synthesis is currently an area of considerable interest, especially in the area of catalysis, where the bimetallic nanoparticles often posses greater catalytic activity than that of their monometallic counterparts. Much work has been carried out in creating Au–Pd and Au–Pt

alloys, given the relatively low reactivity of gold and the high selectivity that these catalysts posses in a wide variety of reactions, including hydrogenation (Toshima et al. 1992) and acetylene cyclisation (Schmid et al. 1991). Colloidal gold particles did not become the subject of scientific study until the work of Michael Faraday in the 1850́s (Faraday 1857) but have been reported as far back as 1612 as a means of staining glass (Neri 1629). Current areas of interest as to potential uses of gold nanoparticles include nanoelectronic devices (using bacteria) (Berry and Saraf 2005), self-assembled thin films (Chumanov et al. 1996) and as a potential tool for DNA labelling (Elghanian et al. 1997; Merkoçi et al. 2005; Merkoçi 2007), an area of much interest as NP labels present none of the associated health or waste disposal issues as their radioactive counterparts. Several applications of gold nanoparticles for DNA (Pumera et al. 2005; Castañeda et al. 2007) and protein (Ambrosi et al. 2007) sensing have been reported by our group. For the case of silver, a number of interesting optical properties arise from the size and shape dependence of the position and shape of the Plasmon absorption band, in addition to the absence of d-band transitions, which can overlap with the free-electron contribution in the case of gold (Brust and Kiely 2004). Silver particles are also reported to give a greater Raman enhancement (Vlčková et al. 1996). The well known anti-bacterial properties of silver have directed research towards the development of new processes to make new antibacterial fabrics (Tarimala et al. 2006) and engineering new methods to inhibit microbial activity (Nomiya et al. 2004).

There are many known methods of NP preparation. Most reported methods detail the reduction of a metal salt by a suitable reducing agent, and by carefully controlling the reagents and reaction conditions, it is possible to direct NP formation to give a specific final size and/or shape. Novel methods, which are recently published use biosynthetic pathways and plant extracts to direct size and shape (Huang et al. 2007). For Au–Ag alloy clusters, two main preparation methods exist, an evaporation and condensation procedure reported by Papavassiliou (1976) or via a method whereby metal ions are reduced under specific conditions. Recently, Au particles and nano-rods have been synthesized from Ag seeds (Xu et al. 2007).

In this report, we aim to examine a simple synthetic strategy for producing Ag and AuNPs by reduction of the metal salts $AgBF_4$ and $HAuCl_4$ by $NaBH_4$ in water. Methods for producing Au–Ag and Ag–Au alloy clusters are also examined, where the morphology is determined by the order of reactant addition.

The obtained NPs are characterized by transmission electronic microscopy (TEM) and UV–Vis absorption spectroscopy, so as to evaluate their qualities. Moreover, a direct electrochemical detection protocol that involves the use of glassy carbon electrode is also applied to characterize the prepared NPs. Cyclic voltamperometry that allows a simple and fast detection and quantification of either silver or gold NPs is used. The developed NPs and the related electroanalytical method seem to be with interest for future sensing and biosensing applications including DNA sensors and immunosensors.

Experimental

Reagents and materials

Silver tetraflouroborate 98%, was purchased from Aldrich. Hydrogen tetrachloroaurate (III) hydrate 99.9%, was purchased from Strem Chemicals and sodium borohydride powder >98.5% was purchased from Sigma-Aldrich. Milli-Q water from ELGA Labwater system was used. Analytical grade (Merck) HCl and NH_3 and ultra-pure water have been used for the electrochemical measurements. All reagents were used as received without any further purification. All glassware and magnetic stirrers were cleaned with *aqua regia* followed by copious rinsing with de-ionized water.

Electrochemical measurements were carried out at room temperature in a 900 μl cell with a three electrode configuration. A glassy carbon electrode (GCE, (CH Instruments, Austin, TX, USA) with 2 mm of surface diameter (area: 3.14×10^{-2} cm^2), was used as working electrode. Prior to use, the surface of the electrode was polished with alumina paper (polishing strips 301044-001, Orion, Spain) and rinsed carefully with bi-distilled water. A Selecta ultrasonic bath was used to clean the GCE surface. A platinum wire as counter electrode and an Ag/AgCl double junction electrode, with an internal solution of potassium chloride saturated, reference electrode were used in the three electrodes configuration. A magnetic stirrer from

Science Basic Solutions (Spain) was used for the deposition/conditioning steps.

Instruments

UV-VIS Spectroscopy measurements were performed using a UV-Unicam 5625 UV-VIS spectrometer and 10 mm quartz cuvettes.

Transmission electron Microscopy (TEM) was performed using a JEOL JEM 2011 (Jeol Ltd Tokyo, Japan) operating at an accelerating voltage of 200 kV. Samples were prepared by placing a drop of the nanoparticle solution on a 3 mm copper grid covered with carbon film. Excess film was removed with absorbent paper.

A centrifugal from Fisher Bioblock Scientific-Sigma (Germany) was used for the nanoparticles purification.

Electrochemical measurements were performed with a Compactstat potentiostat (Ivium Technologies-The Netherlands) interfaced to a personal computer.

Synthesis of nanoparticles

Synthesis of silver nanoparticles (AgNP)

Water-dispersible unprotected AgNPs have been prepared based on a method reported earlier by Dirk et al. (1998), which involved the reduction of silver perchlorate by sodium borohydride. The procedure outlined below is adapted from the above but using the metal salt $AgBF_4$ in place of $AgClO_4$, to see what effect (if any) changing of the anion has on NP characteristics such as size and shape.

Briefly, a typical experiment involved the required amount (usually from 1 μL to 5.08 mL, 0.295 M) of freshly prepared ice-cold aqueous $NaBH_4$ being added, under vigorous stirring, to 100 ml of Milli-Q water in an ice bath. To this, the required amount of $AgBF_4$ solution (from 1 μL to 5 mL, 0.1 M) was then added as quickly as possible via a syringe. The reaction was left under vigorous stirring for 40 min, to ensure that it continued to completion. The AgNPs were then stored in darkness to prevent precipitation.

Synthesis of Ag–Au nanoparticles (Ag–AuNPs)

The Ag–AuNP solution was prepared by reaction of a previously prepared AgNP solution (a 50 mL aliquot) with a 0.01 M $HAuCl_4$ stock solution, so as to ensure concentration ratios (Ag/Au ions): 2:1; 1:1 and 1:2.

The required volumes of $HAuCl_4$ solution (0.25, 0.5 and 1 mL from 0.01 M) were added drop wise to the 50 mL AgNP aliquots in an ice bath. The solutions were allowed to stir for 30 min to ensure complete reaction. The Ag–AuNPs were then stored in darkness to prevent precipitation.

Synthesis of gold nanoparticles

The AuNP solution was prepared by adapting the previous report for the synthesis of AgNPs (sect. "Synthesis of Silver Nanoparticles (AgNP)"). Briefly, a red solution of AuNPs (representing a $HAuCl_4$ concentration of 1×10^{-4} M) was prepared first by rapid injection of 1 mL 0.01 M $HAuCl_4$ solution into 100 mL of ice-cold milli-Q water containing 3×10^{-4} L of 0.295 M $NaBH_4$ solution, then allowed to stir for 40 minutes to ensure the reaction had continued to completion. The AuNPs were then stored in darkness to prevent precipitation.

Synthesis of Au–Ag nanoparticles (Au–AgNPs)

To a 100 mL AuNP solution as prepared above (sect. "Synthesis of gold nanoparticles"), 50 μL of 0.1 M $AgBF_4$ solution was added rapidly and the solution was left to stir in an ice bath for 30 min. The Au–AgNPs were then stored in darkness to prevent precipitation.

Electrochemical detection of NPs

Cyclic voltammetry was the electrochemical technique used for the electrochemical detection of NPs. Before the electrochemical measurements, NPs solutions in appropriate electrolytes media were prepared. The electrolytes used were NH_3 1 M in the case of the AgNPs and HCl 0.1 M for the AuNPs detection.

AgNPs electrochemical detection was performed by immersing the three electrodes system in a stirred solution of AgNPs in NH_3 1 M, and applying a potential of −0.80 V for 60 s. After that, cyclic voltammograms were scanned from −0.80 V to + 0.30 V at a scan rate of 50 mV s^{-1}.

In the case of AuNPs, the electrodes (the same as for AgNPs) were immersed in a stirred solution of AuNPs in HCl 0.1 M and held at a potential of −0.80 V for 240 s. Then, an anodic scan was performed from −0.80 V to +1.30 V, at a scan rate of 50 mV/s. The silver and gold oxidations are observed at +0.10 and +0.95 V, respectively and constitute the analytical signals.

The negative conditioning potential is necessary in both cases to reduce the possible metal oxides on the surface of the nanoparticles and assure the maximum re-oxidation signal—the measuring signal—during the stripping step.

To prove that in all cases the analytical signal corresponds to nanoparticles and not to possible excess of metallic ions from the synthesis solutions, aliquots of 2 ml of these solutions were centrifuged at 14,000 rpm for 30 min and then the supernatant was separated from the precipitated nanoparticles. The supernatant solutions were mixed with the appropriate electrolyte and measured in the same way as the NPs solutions.

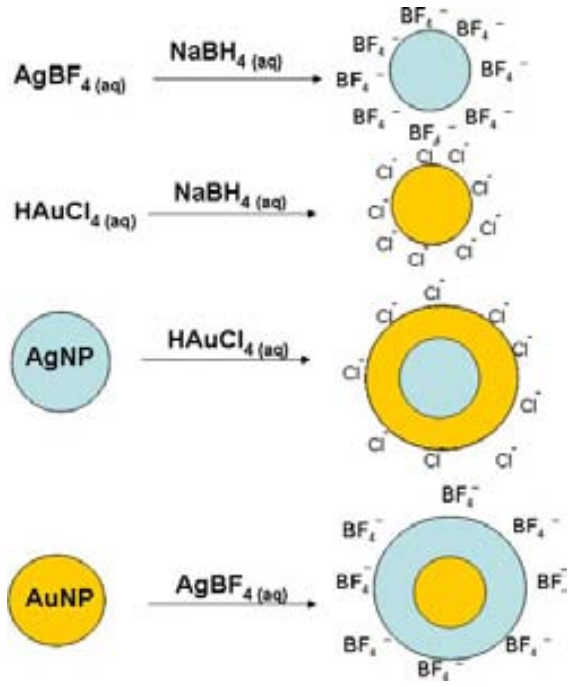

Fig. 1 Schematic (not in scale and shape) detailing of the synthesis of different nanoparticles

Results and discussion

Nanoparticle generation

Four kinds of nanoparticles: AgNP, AuNP, Ag–AuNP and Au–AgNP have been synthesized and characterized using different techniques. Figure 1 is a schematic of the synthesis principles applied for each NP.

AgNP generation

The AgNP generation method proposed, avoid the use of $AgNO_3$ as silver precursor, since the presence of the NO_3^- oxidant anion on the surface of the AgNP formed could harm their future applications as labels for affinity biosensors.

Upon injection of the silver ions (as $AgBF_4$) into the ice-cold $NaBH_4$ solution, an initial aggregation stage was visible, represented by a darkening in the solution. This darkening lasted only a fraction of a second before the solution became clear again. As argued by Dirk et al. this initial aggregation could be due to the presence of small (1−3 nm), borohydride bound particles of silver. These clusters grow by an aggregative mechanism to their final sizes, giving rise to the colour changes observed.

The effect of silver ions concentration on the AgNP size was studied first (see Supporting Information for details on the experiment performed). It can be seen that an increase in $AgBF_4$ concentration increases both the maximum size and the range of sizes adopted by the nanoparticles formed.

The final colour of the solution after 40 min stirring was dependant on the concentration of silver ions, as shown in Fig. 2A.

The silver content of vial (a) was found to precipitate out of the solution after a few hours, as can be seen from the picture. It is proposed that this concentration ($5{\cdot}10^{-3}$ M) represents the upper limit of AgNP stability; the silver is concentrated to such an extent that it will readily aggregate and precipitate after a few hours. Vial (b) was seen to contain a turbid solution that was an orange/green colour, and opaque, when held up to a light source. Vial (c) was deep orange in colour, with vials (d) and (e) yellow and pale-yellow, respectively. Vials (f–h) did not posses any visible colour, presumably attributed to the low AgNP concentration. Although the silver

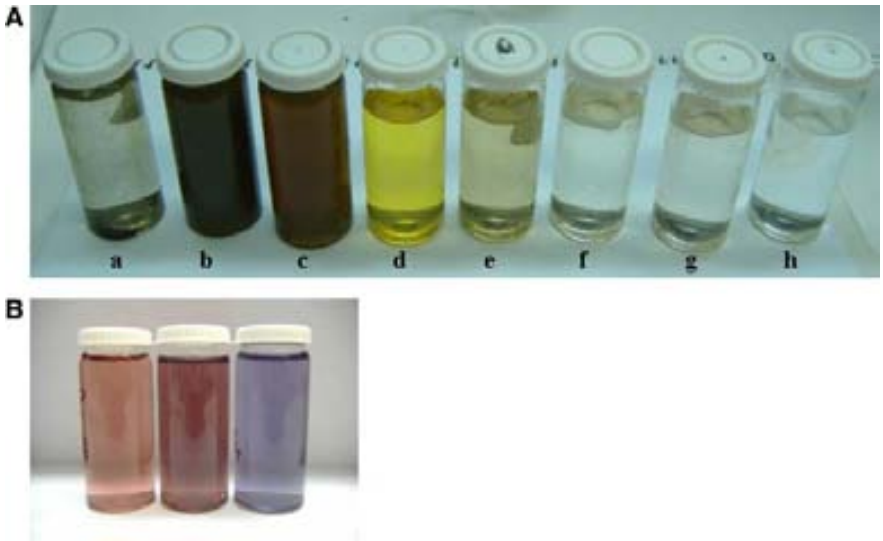

Fig. 2 (**A**) Picture of AgNP solutions prepared using $AgBF_4$ solutions with concentrations of: (a) 5×10^{-3} (b) 1×10^{-3} (c) 5×10^{-4} (d) 1×10^{-4} (e) 5×10^{-5} (f) 1×10^{-5} (g) 5×10^{-6} and h) 1×10^{-6} M. (**B**) Pictures of AuNP solution (left), Au–AgNP solution (middle) and Ag–AuNP solution (right) (concentration of silver salt or gold salt is $1{\cdot}10^{-4}$ M). The NPs are prepared as explained in the text

content of vial (a) precipitated out of solution readily, the others were found to be stable up to 5 months at ambient temperature, if stored from light.

Ag–AuNPs generation

Addition of the yellow $HAuCl_4$ solution to the yellow AgNP aliquots caused an instantaneous colour change from yellow to lilac. After 30 min of stirring, no further colour change occurred to the Ag–AuNPs. An identical lilac colour (Fig. 2B right) was obtained for each of the Ag:Au ratios tested (2:1, 1:1 and 1:2). No precipitation of the particles occurred after 3 months, although after two weeks a darkening from lilac to purple occurred in each of the samples. This darkening could presumably be attributed to NP aggregation, though not to such an extent to cause a complete Ag–AuNP precipitation.

AuNP generation

Upon injection of the Au metal ions (as $HAuCl_4$ solution), no initial aggregation was visible as happened in the AgNP preparation. Instead, the solution became an intense orange colour, which finally darkened gradually to a pale red colour after 40 minutes agitation (Fig. 2B left) indicating the formation of AuNPs.

Au–Ag mixture generation

Injection of a clear $AgBF_4$ solution to the AuNPs solution caused an instantaneous colour change from pale red to a deeper red/purple (Fig. 2B middle) due to the formation of Au–AgNPs. No change in colour was apparent after 3 months of storage, indicating that no nanoparticle aggregation occurred.

Characterization by UV-VIS

AgNPs

The more dilute AgNP solutions samples (representing concentrations 1×10^{-6}–1×10^{-5} M $AgBF_4$) (see supporting information Figure S1) were found to contain a barely visible $\sim$ 400 nm peak, whilst in Fig. 3A (concentrations 1×10^{-4}, 5×10^{-4} and 1×10^{-3} M $AgBF_4$) this peak is visible, increasing in both height and width with increasing silver ion concentration. The 400 nm peak for $1{\cdot}10^{-3}$ M appears very broad with a number of sub-peaks and shoulders, and it is proposed that such a broad peak indicates that there exists a wide range of nanoparticle sizes (Solomon et al. 2007), as can be seen also from the TEM image (Fig. 4Ic). The most concentrated sample (5×10^{-3} M, UV-VIS spectra not supplied) was found not showing any absorption indicating that all the silver ions within have precipitated.

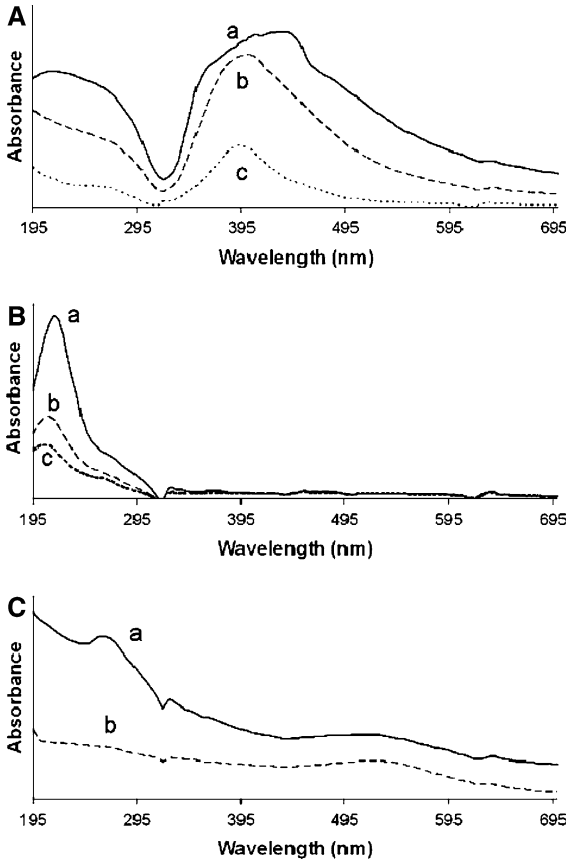

Fig. 3 UV-VIS spectra for: (**A**) AgNPs corresponding to (a) 1×10^{-3}, (b) 5×10^{-4}, (c) 1×10^{-4} M $AgBF_4$ used during the AgNP synthesis. (**B**) Ag–Au NP solutions corresponding to Ag: Au molar ratios (of the 1×10^{-4} M salt solutions) of (a) 1:2, (b) 1:1, (c) 2:1. (**C**) Solutions of (a) Au–Ag NPs of 1:1 Au: Ag molar ratios (of the salt solutions used) and (b) Au NPs corresponding to 1×10^{-4} M $HAuCl_4$ used during the synthesis of AuNPs

Ag–AuNPs

The spectra obtained for the different Ag:Au ratios (see Fig. 3B) show an increase in the intensity of absorbance at 215 nm with an increase in the gold content of the mixture (due to the increasing concentration of $HAuCl_4$). When Figure S1 (UV-VIS spectra of the 325 – 600 nm region for Ag–Au NPs) is compared to the UV–VIS spectra of Fig. 3A, it is apparent that the defined peaks associated with AgNPs at around 400 nm have dramatically decreased in intensity, indicating the possible loss of Ag nanoparticle character (concerning to the Ag surface plasmon).

Au–AgNPs

The spectra obtained for the Au–Ag mixture (see Fig. 3Ca) shows strong absorbance at 275 nm, a peak not apparent in the spectra for the AuNPs (Fig. 3Cb). Absorbance in this range is commonly associated with a silver-borohydride nano-species (see Fig. 3A), although the peaks at 400 nm that we would expect from silver are not apparent. The broad peak visible at 530 nm is a peculiar characteristic of the gold surface plasmon (Grace and Pandian 2006) and is present in both the Au and Au–Ag cases (see Fig. 3C), implying that AuNPs have retained their nanoparticle character after the addition of $AgBF_4$.

The disappearance of the primary bands of AuNPs and AgNPs and the appearance of new bands located at i.e. 215 nm for the Ag–Au NPs, indicates the formation of core-shell composites. The absorption edges show a strong blue shift with respect to bulk Ag or Au materials. This blue shift is an obvious quantum size effect and has been observed in many nanometer-sized semiconductor materials (Sun et al. 2006; Wu et al. 1997).

Characterization by TEM.

TEM spectroscopy of Ag nanoparticles

From Fig. 4I, it can easily be seen that an increase in silver concentration increases the range of sizes adopted by silver nanoparticles. Figure 4Ia (corresponding to $AgBF_4$ concentration 1×10^{-5} M) shows a typical NP: spherical and with a diameter between 15 and 20 nm. Figure 4Ib (corresponding to $AgBF_4$ concentration 1×10^{-4} M) shows a number of NPs with diameters of approximately up to 20 nm. Figure 4Ic (corresponding to $AgBF_4$ concentration 1×10^{-3} M) shows the range of particle size visible in the most concentrated sample. Nanoparticles with diameters ranging from 5 to 40 nm are present. These larger particles, with diameters >20 nm, were found to be surrounded by a large number of $\sim$5 nm particles. This finding is supported by the UV-VIS spectra (Fig. 3A) showing a very broad 400 nm peak, which is indicative of a wide range of nanoparticle size. It can be seen that the larger nanoparticles generally do not adopt a spherical shape; instead an elongated form is preferred. This longer shape could

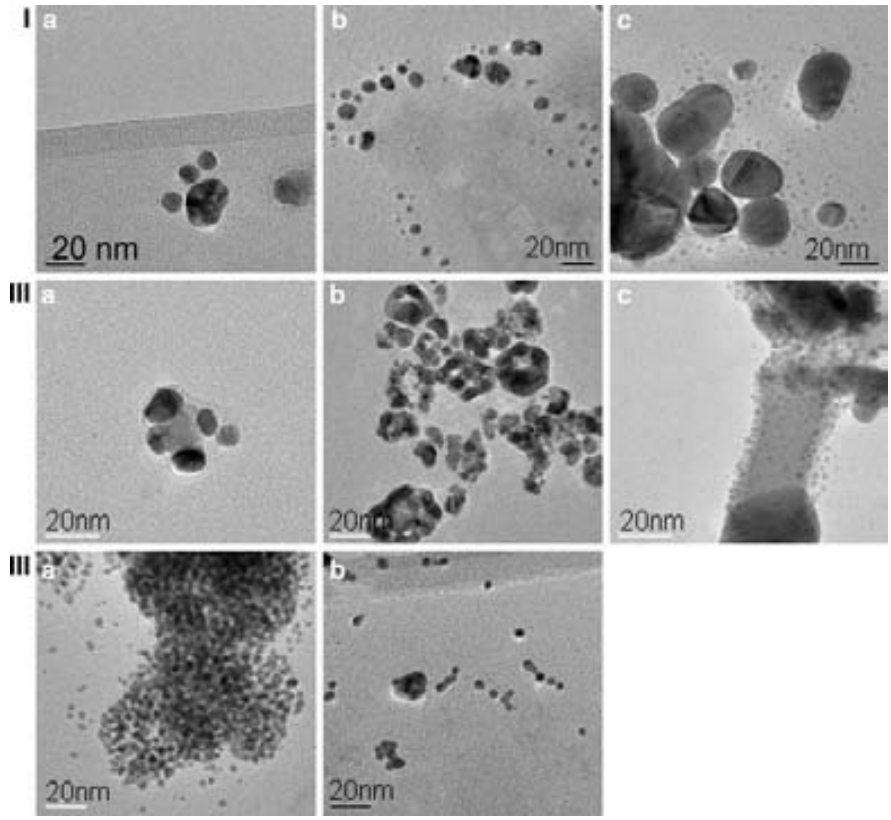

Fig. 4 TEM images of (**I**) AgNPs obtained from (a) 1×10^{-5} (b) 1×10^{-4} and (c) 1×10^{-3} M $AgBF_4$. (**II**) TEM images of Ag–Au NPs with Ag: Au ratios of (a) 2:1 (b) 1:1 (c) 1:2. (**III**) TEM image of (a) Au NPs and (b) Au–Ag NPs of 1:1 Au:Ag. Other experimental conditions of NP preparation as described in the text

be due to the aggregation of two or more particles together. The smaller 5 nm particles are generally more rounded, adopting a spherical shape like that of the NPs found in the lesser concentrated samples. It is also interesting to note that such extremes of particle size can only be found in the 1×10^{-3} M sample, in the others the particles were found generally of the same size. These smaller particles could only be found surrounding the larger 20 nm and above particles, implying that they could perhaps in some way be attracted to these larger particles, by means of electrostatic interactions. Additional AgNP TEM images (corresponding to $AgBF_4$ concentrations 1×10^{-5}, 1×10^{-4} and 1×10^{-3} M) can be found in the supporting information, Figure S2.

TEM spectroscopy of Ag–Au nanoparticles

It can be seen (see Fig. 4II) that an increase in Au concentration causes an increase in AgNP agglomeration. Figure 4IIa (corresponding to Ag:Au ratio 2:1) shows agglomeration of 4 AgNPs held together by an apparently lighter grey coloured substance between them, which is presumably a form of gold formed by reduction of $HAuCl_4$. Figure 4IIb (corresponding to Ag:Au ratio 1:1) shows aggregation of Ag nanoparticles to a much greater degree; a number of large "wheel" like structures can be seen, each consisting of separate AgNPs joined together. The formation mechanism of such circular formations is still unclear. One proposed mechanism could be similar to that proposed by Kim et al. for the formation of hollow nanoframes (Kim et al. 2007), whereby the AgNP is disrupted by the presence of Au, causing the Ag cluster to fall apart and Au to fill the spaces thus created. This fact would explain that the size of AgNPs in these "wheels" is smaller than in Ag–AuNPs with lower Ag:Au ratio (Fig. 4IIa). The final image, Fig. 4IIc**,** (corresponding to Ag:Au ratio 1:2) shows the presence of a number of different sizes of AgNP, with the larger particles apparently surrounded by the same light grey coloured material that could be seen in Fig. 4IIa. In addition to this, a number of much smaller (<5 nm) particles can also be seen, surrounding the dark Ag particle. It is not clear whether these smaller particles are of gold or silver, the presence of gold nanoparticles requiring that

the $HAuCl_4$ ions are reduced, although no further $NaBH_4$ was added after the injection of $HAuCl_4$. This reduction could only be possible by those BH_4^- ions remaining in solution or by those bound to the surface of the AgNP. To test this, an Ag–Au mixture was prepared again, but this time the AgNPs were left for 24 h before $HAuCl_4$ was added, as several studies (Davis and Swain 1960; Davis et al. 1962) have shown that BH_4^- ions in water will decompose into non reductive species, as indicated in the equation below:

$$BH_4^- + H^+ + 2H_2O \rightarrow \text{intermediate} \rightarrow HBO_2 + 4H_2$$

Upon $HAuCl_4$ injection, the same colour change as before occurred, indicating the formation of a similar chemical species as before. These results imply that $HAuCl_4$ is reduced by the BH_4^- ions found on the AgNP surface, rather than those free in solution as we expect these free ions to have decomposed in the time between $NaBH_4$ addition and the addition of $HAuCl_4$. A galvanic replacement reaction similar to the described one by Lu et al. (2007) between the added Au(III) and Ag(0) of the NPs surface is also possible:

$$Au(III) + 3Ag(0) \rightarrow 3Ag^+ + Au(0)$$

In a similar mode, nearly monodisperse hollow gold nanospheres have been reported to be synthesized by sacrificial galvanic replacement of cobalt nanoparticles (Schwartzberg et al. 2006).

The additional images (Figure S3) present in the supporting information reveal the presence of a number of triangular NP formations, consisting of a number of different Ag–Au subunits. Figure 5A shows the microanalysis result of the Ag–AuNP (1:1) mixture, with traces of both silver and gold present, taken from the middle of one of the "wheel" structures. By the above mentioned method of Kim et al. this would imply that the AgNPs form the 'rim' of the wheel and the addition of $HAuCl_4$ forms the 'spokes'.

TEM spectroscopy of Au nanoparticles

As seen from Fig. 4IIIa, the AuNPs prepared by the above method were found to be spherical and typically 3–5 nm in size. The AuNPs were found to exist in large and often circular clusters varying in size from several tens to several hundreds of particles. Individual AuNPs could not be found separate from these large clusters, implying that some

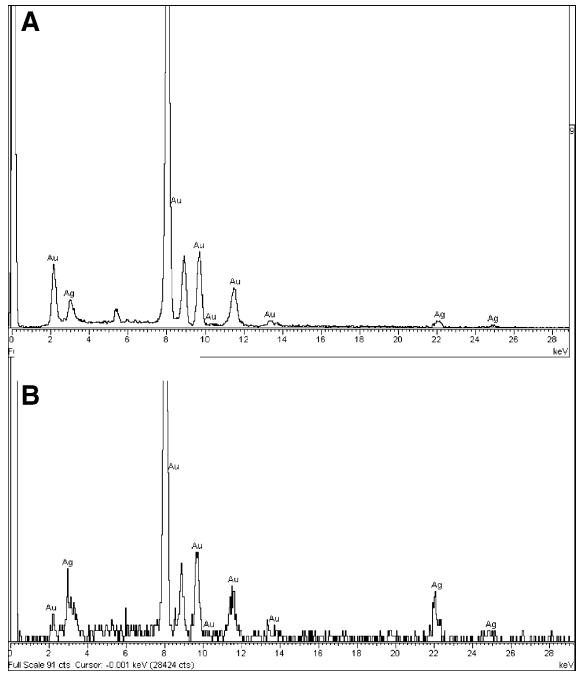

Fig. 5 Microanalysis results of (**A**) Ag–Au NPs corresponding to 1:1 Ag: Au ratio and (**B**) Au–Ag NPs corresponding to 1:1 Au: Ag ratio showing presence of both gold and silver in the NP formed. (See corresponding table at Supporting Information)

electrostatic force could be responsible for keeping them held together. Additional TEM imaging of these AuNP clusters can be found in the Supporting information (see Figure S4).

TEM spectroscopy of Au–Ag nanoparticles

Figure 4IIIb shows the species resulting from addition of $AgBF_4$ to a solution of AuNPs. The large AuNP clusters were found to be completely disrupted and a number of the smaller AuNPs can be seen to have agglomerated together, though not to the extent seen in some of the Ag–Au mixtures. There is no evidence to support the formation of AgNPs. The microanalysis results (Fig. 5B) show only a slight amount of silver is present. It appears that, the only effect silver addition has had was to disrupt the AuNP clusters, with the overall shapes and sizes of the Au–AgNPs not vastly different from that of the AuNPs. Additional TEM imaging of these Au–AgNP clusters can be found in the Supporting information (see Figure S5).

Electrochemical characterizations

To confirm the possibility for future applications of the developed nanoparticles for sensors, their electrochemical characterization was performed. Figure 6 shows cyclic voltammograms in 1 M NH_3 obtained for a 25 μM AgNPs solution (black curve), the supernatant solution after centrifugation (grey curve) and for the electrolyte (blank-dot line). It can be observed that the current peak corresponds to the oxidation of the silver at approximately +0.10 V for the AgNPs solution. The supernatant solution does not exhibit any peak, so can be assured that the entire signal observed corresponds to NPs and not to possible excess of silver ions from the synthesis solution.

In the case of the AuNPs, cyclic voltammograms were registered in 0.1 M HCl, for a 50 μM AuNPs solution (black curve), the supernatant solution after centrifugation (grey curve) and for the electrolyte (blank-dot line), as it is shown in Fig. 7. A peak at approximately +0.95 V is observed for the AuNPs solution, which corresponds to the oxidation process of gold. A smaller peak for the supernatant solution also appears. Two facts could explain this behaviour. The centrifugation step is not efficient due to the smaller size of the NPs that stay in the supernatant solution (the solution remains slightly coloured). On the other hand, the peak could be, due to the presence of an excess of gold ions from the synthesis solution.

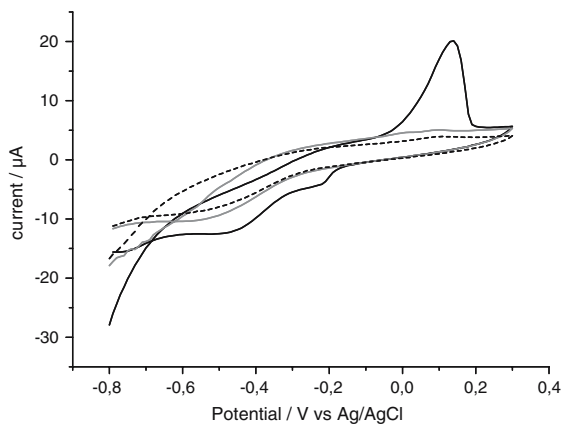

Fig. 6 Cyclic voltammograms recorded in 1 M NH_3, from −0.80 V to +0.30 V, for a 25 μM AgNPs solution (black curve), the supernatant solution after centrifugation (grey curve) and for the electrolyte solution (blank-dot line). Deposition/conditioning potential: −0.8 V; deposition/conditioning time: 60 s; scan rate: 50 mV/s

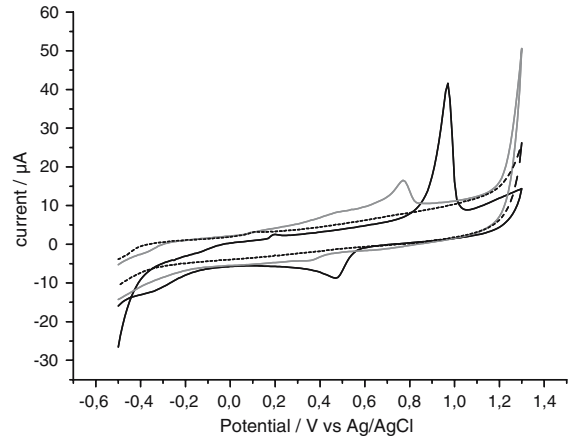

Fig. 7 Cyclic voltammograms recorded in 0.1 M HCl from −0.80 V to +1.30 V, for a 50 μM AuNPs solution (black curve), the supernatant solution after centrifugation (grey curve) and for the electrolyte solution (blank-dot line). Deposition/conditioning potential: −0.8 V; deposition/conditioning time: 240 s; scan rate: 50 mV/s

The CVs obtained for both nanoparticles show that it is possible to use these nanoparticles for sensing applications. Moreover, some preliminary results (not shown) from the signals obtained from the corresponding core-shell nanoparticles indicate the possibility for their future applications in biosensing of DNA and proteins in a similar way as reported recently by our group (Pumera et al. 2005; Castañeda et al. 2007; Ambrosi et al. 2007).

Conclusions

Four kinds of water-soluble nanoparticles: AgNP, AuNP, Ag–AuNP and Au–AgNP have been synthesized and characterized using transmission electronic microscopy (TEM), UV-Vis absorption spectroscopy and cyclic voltammetry. The reported nanoparticles show stability in water suspensions up to several months of storage, indicating that no nanoparticle aggregation occurred.

An important point we observe here is that the morphologies of the obtained nanoparticles are determined by the order of addition of reactants beside the other experimental conditions such as the metal ion concentration, and other appropriate parameters, as was seen by the TEM and UV studies.

The electrochemical characterizations performed by using cyclic voltammetry show significant responses for

both silver and gold nanoparticles in terms of well defined and sensitive oxidation currents responses with interest for future applications in sensors.

More quantitative studies on these aspects are currently in progress.

Acknowledgments This work is supported by Projects: MAT2005-03553 and Consolider-Ingenio 2010, Project CSD2006-00012. CTQ2007-63913

References

Ambrosi A, Castañeda MT, Killard AJ, Smyth MR, Alegret S, Merkoçi A (2007) Double-codified gold nanolabels for enhanced immunoanalysis. Anal Chem 79:5232–5240

Berry V, Saraf RF (2005) Self-assembly of nanoparticles on live bacterium: an avenue to fabricate electronic devices. Angew Chem Int Ed 44:6668–6673

Brust M, Kiely CJ (2004) Monolayer protected clusters of gold and silver. Colloid Colloid Assemblies 3:96–119

Castañeda MT, Merkoçi A, Pumera M, Alegret S (2007) Electrochemical genosensors for biomedical applications based on gold nanoparticles. Biosens Bioelectron 22:1961–1967

Chumanov G, Sokolov K, Cotton TM (1996) Unusual extinction spectra of nanometer-sized silver patricles arranged in two-dimensional arrays. J Phys Chem 100:5166–5168

Davis RE, Swain CG (1960) General acid catalysis of the hydrolysis of sodium borohydride. J Am Chem Soc 82:5949–5950

Davis RE, Bromels E, Kibby CL (1962) Hydrolysis of sodium borohydride in aqueous solution. J Am Chem Soc 84:885–892

Dirk L, Hyning V, Zukoski CF (1998) Formation mechanisms and aggregation behavior of borohydride reduced silver particles. Langmuir 14:7034–7046

Elghanian R, Storhoff JJ, Mucic RC, Letsinger RL, Mirkin CA (1997) Selective colorimetric detection of polynucleotides based on the distance-dependent optical properties of gold nanoparticles. Science 277:1078–1081

Faraday M (1857) Experimental relations of gold (and other metals) to light. Philos Trans R Soc London 147:145–181

Grace AN, Pandian K (2006) One pot synthesis of polymer protected gold nanoparticles and nanoprisims in glycerol. Colloid Surf A: Physicochem Eng Aspect 290:138–142

Huang JL, Li QB, Sun DH (2007) Biosynthesis of silver and gold nanoparticles by novel sundried *Cinnamomum camphora* leaf. Nanotechnology 18:Art. No. 105104

Kim D, Park J, An K, Yang NK, Park JG, Hyeon T (2007) Synthesis of hollow iron nanoframes. J Am Chem Soc (Communication) 129:5812–5813

Lu X, Tuan HY, Chen J, Li ZY, Korgel BA, Xia Y (2007) Mechanistic Studies on the galvanic replacement reaction between multiply twinned particles of Ag and $HAuCl_4$ in an organic medium. J Am Chem Soc 129:1733–1742

Merkoçi A (2007) Electrochemical biosensing with nanoparticles. FEBS J 274:310–316

Merkoçi A, Aldavert M, Marín S, Alegret S (2005) New materials for electrochemical sensing. V. Nanoparticles for DNA labeling. Trend Anal Chem 24:341–349

Mulvaney P (1996) Surface plasmon spectroscopy of nanosized metal particles. Langmuir 12:788–800

Neri A (1629) L'Arte Vetraria. Florence 7:129

Nomiya K, Yoshizawa A, Tsukagoshi K, Kasuga NC, Hirakawa S, Watanabe SJ (2004) Synthesis and structural characterization of silver(I), aluminium(III) and cobalt(II) complexes with 4-isopropyltropolone (hinokitiol) showing noteworthy biological activities. Action of silver(I)-oxygen bonding complexes on the antimicrobial activities. J Inorg Biochem 98:46–60

Ozin GA (1992) Nanochemistry: synthesis in diminishing dimensions. Adv Mater 4:612–649

Papavassiliou GC (1976) Surface plasmons in small Au–Ag alloy particles. J Phys F: Metal Phys 6:103–105

Pumera M, Castañeda MT, Pividori MI, Eritja R, Merkoçi A, Alegret S (2005) Magnetically trigged direct electrochemical detection of DNA hybridization based Au67 Quantum Dot—DNA—paramagnetic bead conjugate. Langmuir 21:9625–9629

Schmid G (1992) Large clusters and colloids. Metals in the embryonic state. Chem Rev 92:1709–1727

Schmid G, Lehnert A, Malm JO, Bovin JO (1991) Experimental relations of gold (and other metals) to light. Angew Chem Int Ed 30:874–876

Schwartzberg AM, Olson TY, Talley CE, Zhang JZ (2006) Synthesis, characterization, and tunable optical properties of hollow gold nanospheres. J Phys Chem B 110:19935–19944

Solomon SD, Bahadory M, Jeyarajasingam AV, Rutkowsky SA (2007) Synthesis and study of silver nanoparticles. J Chem Educ 84:322–325

Sun L, Wei G, Song Y, Liu Z, Wang L, Li Z (2006) Solution-phase synthesis of Au@ZnO core-shell composites. Mater Lett 60:1291–1295

Tarimala S, Kothari N, Abidi N, Hequet E, Fralick J, Dai LL (2006) New approach to antibacterial treatment of cotton fabric with silver nanoparticle-doped silica using a sol-gel process. J Appl Polym Sci 101:2938–2943

Toshima N, Harada M, Yamazaki Y, Asakura K (1992) Catalytic activity and structural analysis of polymer-protected Au–Pd bimetallic clusters prepared by the simultaneous reduction of $HAuCl_4$ and $PdCl_2$. J Phys Chem 96:9927–9933

Vlčková B, Gu XJ, Tsai DP, Moskovits M (1996) A microscopic surface-enhanced Raman Study of a single adsorbate-covered collodial silver aggregate. J Phys Chem 100:3169–3174

Wu X, Zou B, Xu J, Yut B, Tang G, Zhang G, Cheng W (1997) Structural characterization and optical properties of nanometer-sized SnO_2 capped by stearic acid. Nanostruct Mat 8:179–189

Xu ZC, Shen CM, Xiao CW (2007) Wet chemical synthesis of gold nanoparticles using silver seeds: a shape control from nanorods to hollow spherical nanoparticles. Nanotechnology 18:Art. No. 115608

SUPPORTING INFORMATION

SILVER, GOLD AND THE CORRESPONDING CORE SHELL NANOPARTICLES FOR SENSING APPLICATIONS

Fraser Douglas[1], Ramon Yañez, Josep Ros

Unitat de Química Inorgànica, Departament de Química, Universitat Autònoma de Barcelona, 08193 Bellaterra, Catalonia, Spain

Sergio Marín, Alfredo de la Escosura, Salvador Alegret, Arben Merkoçi*

Nanobioelectronics & Biosensors Group, Institut Catala de Nanotecnologia, Bellaterra, Catalonia, Spain; Group of Sensors & Biosensors, Departament de Química, Universitat Autònoma de Barcelona, 08193 Bellaterra, Catalonia, Spain

[1]. On leave from: Chemistry Department, University of Glasgow, Glasgow G12 8QQ, UK

*Corresponding author. E-mail: arben.merkoci.icn@uab.es

Effect of silver ions concentration on AgNP size

Eight experiments were run to investigate the effect of silver ions concentration on AgNP size. The concentration of Ag was increased as indicated in **Table 1** below, and the molar ratio $[NaBH_4]$ / $[AgBF_4]$ was kept equal to 3 throughout. $AgBF_4$ stock solution concentration: 0.1M. $NaBH_4$ stock solution concentration: 0.295M.

Table 1:

$AgBF_4$ concentration, M / volume	$NaBH_4$ concentration, M / volume
1×10^{-6} / 1 µL	3×10^{-6} / 1 µL
5×10^{-6} M / 5 µL	1.5×10^{-5} / 5.08 µL
1×10^{-5} M / 10 µL	3×10^{-5} / 10.17 µL
5×10^{-5} M / 50 µL	1.5×10^{-4} / 50.85 µL
1×10^{-4} M / 100 µL	3×10^{-4} / 101.69 µL
5×10^{-4} M / 0.5 mL	1.5×10^{-3} / 0.508 mL
1×10^{-3} M / 1 mL	3×10^{-3} / 1.02 mL
5×10^{-3} M / 5mL	1.5×10^{-2} / 5.08 mL

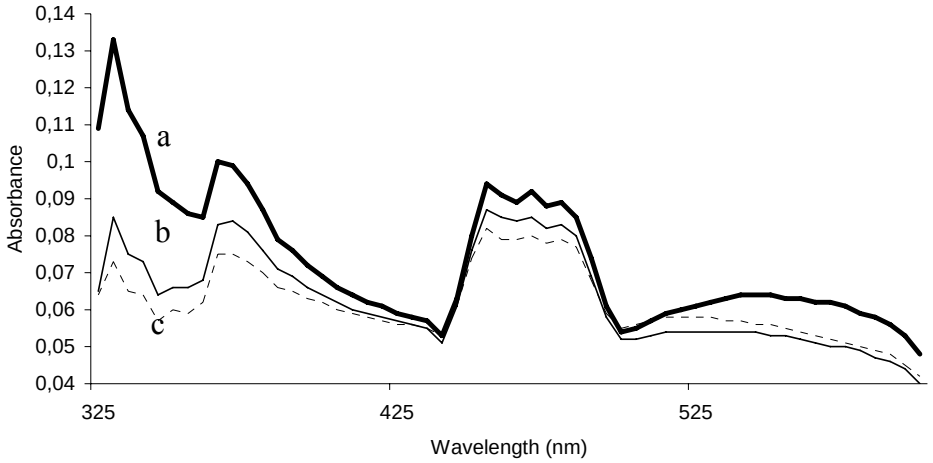

Figure 1: UV-VIS spectra of the 325 – 600 nm region for Ag-Au NPs, with the Ag:Au ratios **a)**1:2 **b)**1:1 **c)**2:1, where it is possible to see the emergence of a number of small peaks with increasing gold concentration.

ADDITIONAL TEM IMAGES

Figure 2: TEM images of AgNPs obtained by using $AgBF_4$ samples at different concentrations

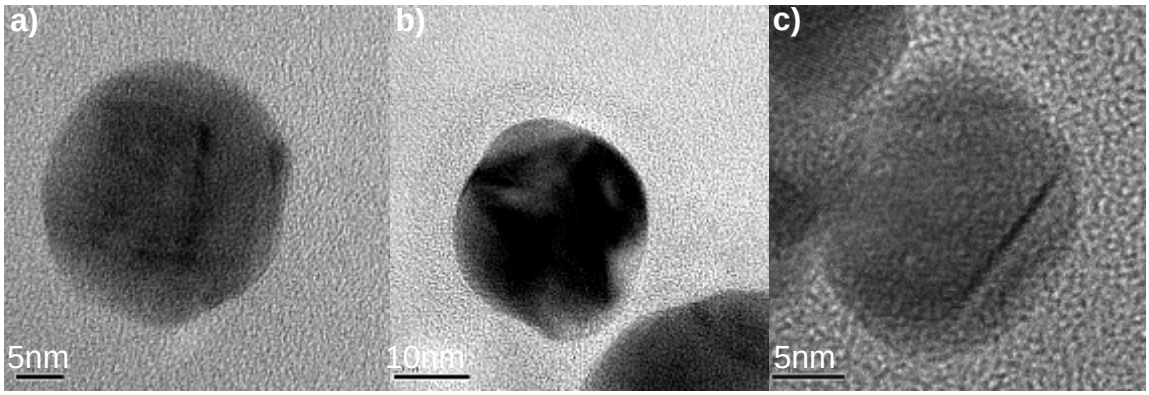

$AgBF_4$ $1x10^{-5}$ M sample.

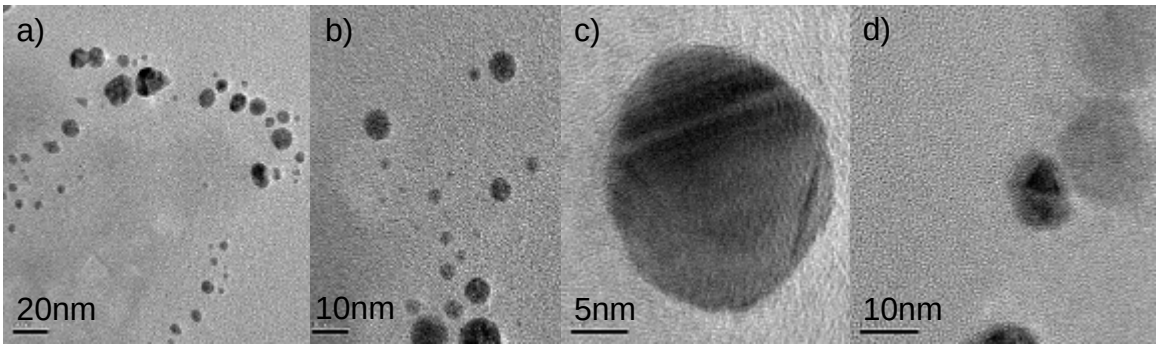

$AgBF_4$ $1x10^{-4}$ M sample.

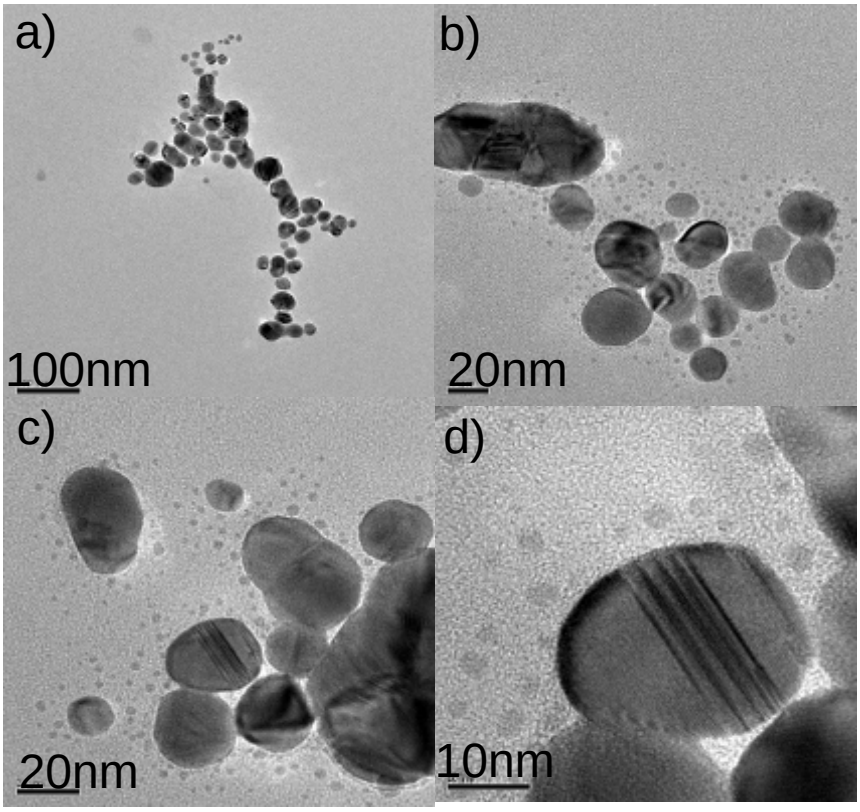

$AgBF_4$ $1x10^{-3}$ M sample.

ADDITIONAL TEM IMAGES

Figure 3: For Ag-Au NP samples

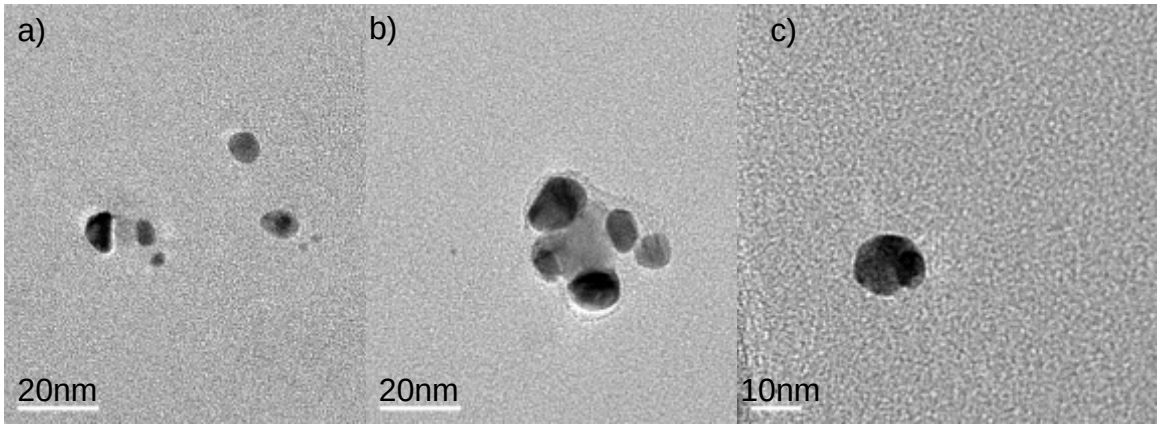

Figure 3.1 TEM images for Ag-Au sample (Ag:Au ratio 2:1)

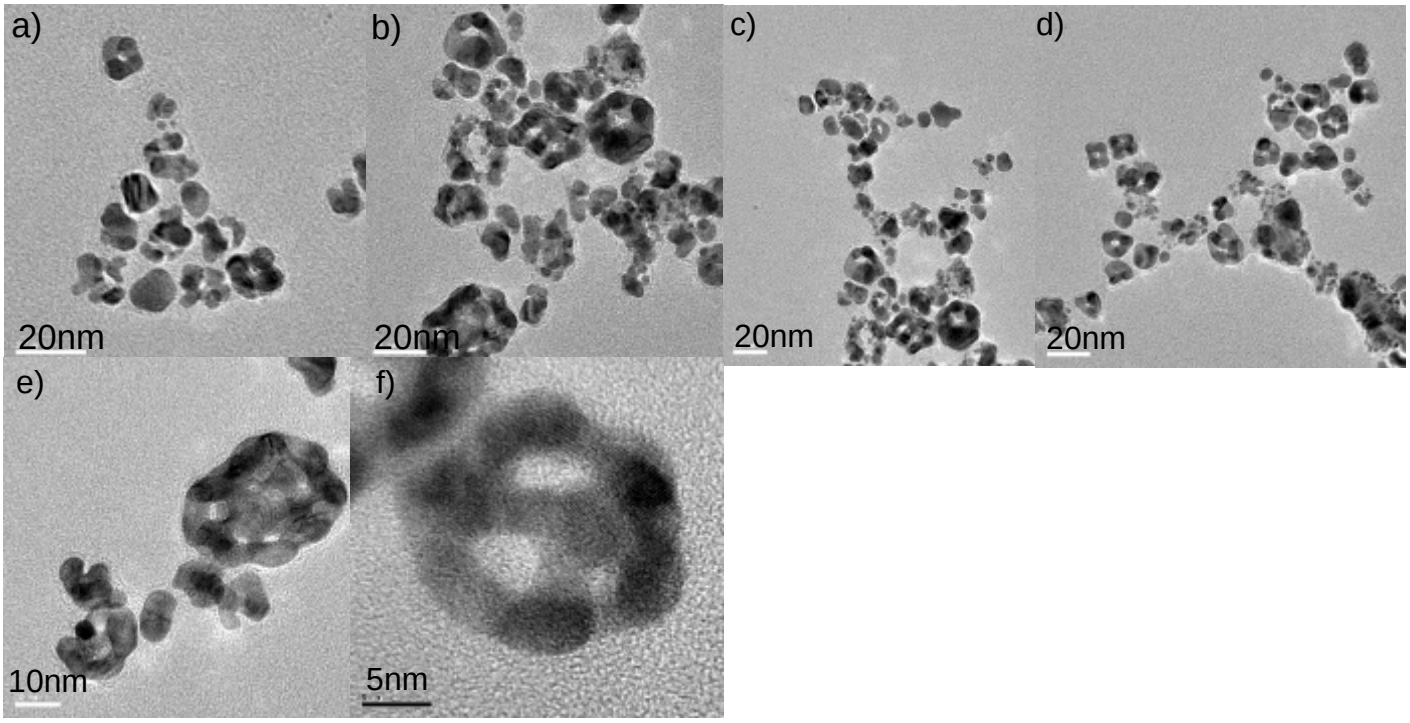

Figure 3.2 TEM images for Ag-Au sample (Ag:Au ratio 1:1)

20nm

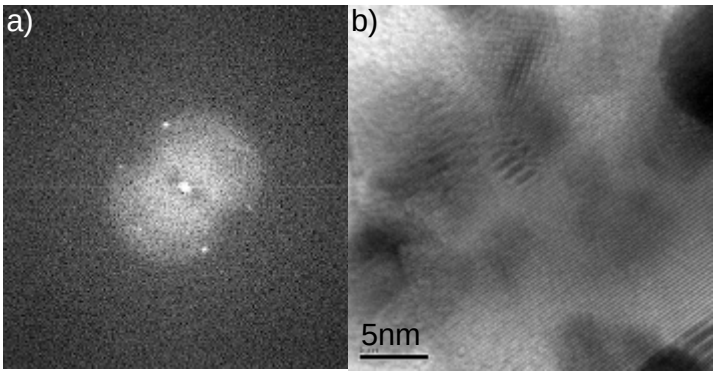

Figure 3.2.1: Electron diffraction pattern a) was obtained from TEM image b) of the central part of a "wheel" structure, hexagonal pattern clearly visible.

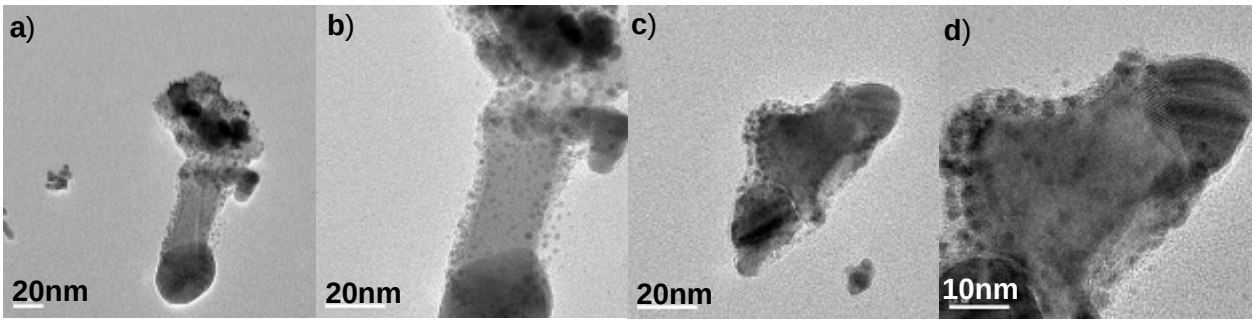

Figure 3.3 TEM images for Ag-Au sample (Ag:Au ratio 1:2)

ADDITIONAL TEM IMAGES

Figure 4: For Au NP sample

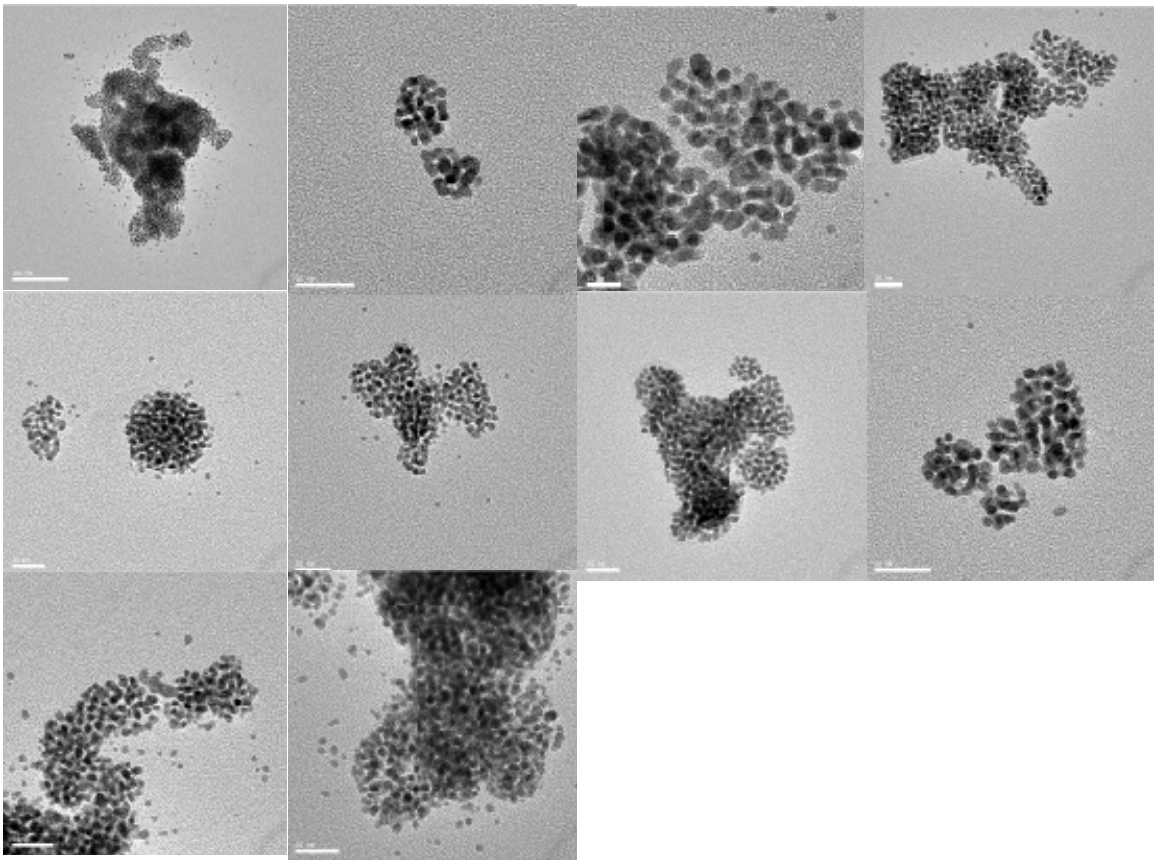

Figure 4: TEM images of some of the Au NP clusters obtained.

Figure 5: For Au-Ag NP samples

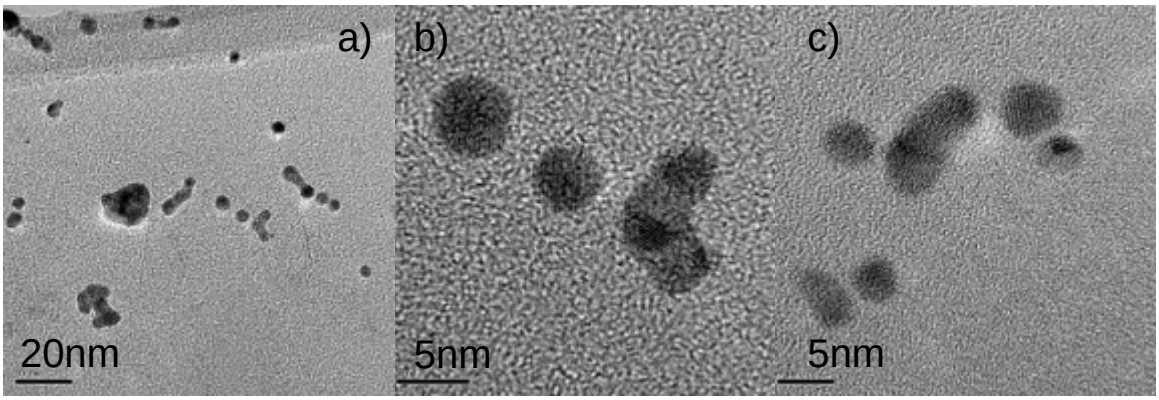

Figure 5: TEM images from Au-Ag sample (Au:Ag ratio 1:1)

Direct electrochemical stripping detection of cystic fibrosis related DNA linked through cadmium sulphide quantum dots

Marín S., Merkoçi A.

Nanotechnology

20, 055101(1-6) (2009)

Nanotechnology **20** (2009) 055101 (6pp) doi:10.1088/0957-4484/20/5/055101

Direct electrochemical stripping detection of cystic-fibrosis-related DNA linked through cadmium sulfide quantum dots

Sergio Marin[1,2] **and Arben Merkoçi**[1,2,3]

[1] Nanobioelectronics and Biosensors Group, Institut Català de Nanotecnologia, Universitat Autònoma de Barcelona, 08193 Bellaterra, Barcelona, Catalonia, Spain
[2] Department of Chemistry, Universitat Autònoma de Barcelona, 08193 Bellaterra, Barcelona, Catalonia, Spain
[3] ICREA, 08010 Barcelona, Catalonia, Spain

E-mail: arben.merkoci.icn@uab.es

Received 23 September 2008, in final form 26 November 2008
Published 9 January 2009
Online at stacks.iop.org/Nano/20/055101

Abstract
Electrochemical detection of a cadmium sulfide quantum dots (CdS QDs)–DNA complex connected to paramagnetic microbeads (MB) was performed without the need for chemical dissolving. The method is based on dropping 20 μl of CdS QD–DNA–MB suspension on the surface of a screen-printed electrode. It is followed by magnetic collection on the surface of the working electrode and electrochemical detection using square-wave voltammetry (SWV), giving a well-shaped and sensitive analytical signal. A cystic-fibrosis-related DNA sequence was sandwiched between the two DNA probes. One DNA probe is linked via biotin–streptavidin bonding with MB and the other one via thiol groups with the CdS QD used as tags. Nonspecific signals of DNA were minimized using a blocking agent and the results obtained were successfully employed in a model DNA sensor with an interest in future applications in the clinical field. The developed nanoparticle biosensing system may offer numerous opportunities in other fields where fast, low cost and efficient detection of small volume samples is required.

S Supplementary data are available from stacks.iop.org/Nano/20/055101

(Some figures in this article are in colour only in the electronic version)

1. Introduction

The enormous amount of information generated in the Human Genome Project has prompted the development of DNA sensors and high-density DNA arrays [1]. DNA hybridization has gained importance as a detection system due to interest in the diagnosis and treatment of genetic diseases, the detection of infectious agents and reliable forensic analysis. Recent activity has focused on the development of hybridization assays that permit simultaneous determination of multiple DNA targets [2, 3].

Conventional and highly sensitive detection methods for DNA are based on labeling techniques using fluorescent dyes [4–6], enzymes [7, 8] or radiolabels [9, 10]. However, since those techniques involve some problems related to stability, a broader range of more reliable, more robust labels that can enable high-throughput bioanalysis and determination of multiple-molecule types present in a sample are now required.

Electrochemical systems for the detection of DNA hybridization based on the use of nanoparticles as tracers have been developed [11–13]. Most of the reported systems are based on stripping voltammetric detection of the dissolved tags [14]. The proposed electrochemical systems are highly promising for rapid, simple and low-cost decentralized detection of specific nucleic acid sequences by DNA hybridization. In addition to the aforementioned advantages, the use of nanoparticles offers 'bar-code' DNA

Table 1. Oligonucleotide sequences used in sandwich system assay.

Probe	Sequence[a]
Capture DNA (CF-A)	5′TGC TGC TAT ATA TAT-biotin-3′
Signaling DNA (CF-B)	Thiol-5′GAG AGT CGT CGT CGT3′
Target DNA (CF-T)[b]	5′ ATA TAT ATA GCA GCA GCA GCA GCA GCA GCA GAC GAC GAC GAC TCT C3′
One-base mismatch (CF-MX1)	5′ ATA TAT AAA GCA GCA GCA GCA GCA GCA GCA GAC GAC GAC GAC TCT C3′
Three-base mismatch (CF-MX3)	5′ ATA TAT CCC GCA GCA GCA GCA GCA GCA GCA GAC GAC GAC GAC TCT C3′
Non-complementary (CF-NC)	5′GGT CAG GTG GGG GGT ACG CCA GG3′

[a] Underlined nucleotides correspond to the mismatches.
[b] Target related to cystic fibrosis gene.

and protein detection [15]. There is a possibility of developing a large number of smart nanostructures with different electrochemical properties that have molecular-recognition abilities and built-in codes for rapid target identification.

The use of QDs as electrochemical labels [16] for DNA offers several advantages with respect to optical properties. In comparison with optical methods, the electrochemical technique is cheaper, faster and easier to use in field analysis. Nanoparticles offer excellent prospects for DNA analysis, owing to their many attractive properties.

Although a nanoparticle-based detection system for DNA hybridization based on magnetically induced electrochemical detection of the cadmium sulfide quantum dot tag linked to the target DNA was reported by Wang *et al* [17], herein we report for the first time a sandwich assay that can directly be detected using a screen-printed electrode.

The proposed method employs lower sample volumes than those reported earlier along with the high sensitivity and fast detection mode.

As far as we know, this is the first time that such a direct electrochemical detection of drop solutions of a CdS DNA sandwich in connection to magnetic microparticles has been presented. Moreover, important aspects related to the avoidance of nonspecific adsorption have been better clarified and the results obtained have been successfully employed in a model biosensor with an interest in future applications. In addition the reported method could be of interest in the development of a portable, automated, multiplexed system for the detection of DNA for use in medical consulting. Such a simple detection device could be an alternative to high cost and sophisticated optical DNA detection systems.

2. Materials and methods

2.1. Apparatus

All voltammetric experiments were performed using a PalmSens (Palm Instrument BV, Houten) that consists of a portable potentiostat interfaced with a palmtop PC (155 mm × 85 mm × 35 mm) (see figure 1, left section). Electrochemical experiments were carried out using a screen-printed electrode (SPE) (Palm Instrument BV, Houten) (see schematic, not to scale, figure 1, right section). The SPE sensors

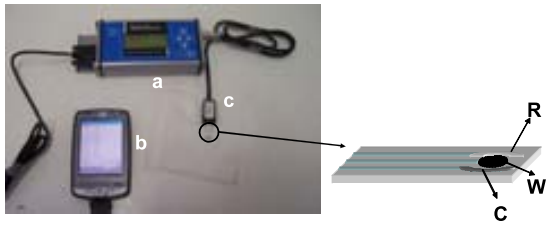

Figure 1. (left) Image of the handheld device system used for CdS QD detection. The principal components are the potentiostat (a), the palm PC (b) and the screen-printed electrodes (SPE) (c). (Right) Schematic of screen-printed electrode formed by the reference (R), working (W) and counter (C) electrodes.

(from the University of Florence—available from Palm Instruments, http://www.palmsens.com) consisted of a screen-printed electrochemical cell with three electrodes in one single strip: a graphite working (W) electrode modified with a plasticizer mixed with mercury acetate, a graphite counter (A) electrode and a silver pseudo-reference electrode (R).

The binding of streptavidin-coated paramagnetic beads with a biotinylated probe and hybridization events were carried out on a TS-100 Thermo Shaker (Spain). Magnetic separation was carried out on an MCB 1200 biomagnetic processing platform (Sigris). A neodymium magnet (diameter 3 mm, height 1.5 mm, Halde Gac Sdad) was used.

2.2. Reagents

All stock solutions were prepared using deionized and autoclaved water. Tris(hydroxymethyl)methylamine (tris), sodium chloride, sodium citrate, ethylenediamine tetraacetic acid disodium salt (EDTA), lithium chloride and Tween 20 were purchased from Sigma-Aldrich. Hydrochloric acid (37%) was purchased from Panreac. Streptavidin-coated paramagnetic beads Dynabeads M-280 Streptavidin (diameter 2.8 μm) were purchased from Dynal Biotech. DNA oligonucleotides were received from Alpha DNA and their sequences are shown in table 1. The CdS-QDs–glutathione, of a size of around 3 nm were synthesized by arrested precipitation of water-dispersed cadmium with hexamethyldisilathiane (HMSDT) as sulfide precursors [18].

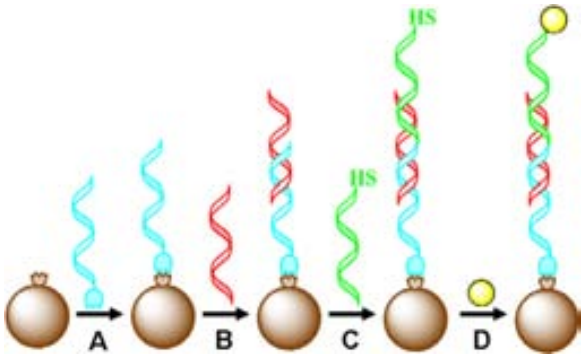

Figure 2. Schematic representation of sandwich protocol (not to scale): (A) immobilization of the biotinylated CF-A probe onto the streptavidin-coated magnetic beads; (B) first hybridization between CF-T and CF-A; (C) second hybridization between CF-T and CF-B modified thiol; (D) addition and capture of the CdS quantum dots.

The buffers and hybridization solution were composed as follows:

- TTL buffer: 100 mM Tris-HCl, pH 8.0; 0.1% Tween 20; and 1 M LiCl.
- TT buffer: 250 mM Tris-HCl, pH 8.0; and 0.1% Tween 20.
- TTE buffer: 250 mM Tris-HCl, pH 8.0; 0.1% Tween 20; and 20 mM Na_2EDTA.
- Hybridization solution: 750 mmol l^{-1} NaCl, 75 mmol l^{-1} sodium citrate.

2.3. Paramagnetic beads' modification and hybridization steps

Figure 2 is a schematic, not to scale, of the MB modification and the hybridization procedures employed for this assay.

Immobilization of the captured DNA probe (CF-A) onto paramagnetic beads. The binding of the biotinylated probe (CF-A) with streptavidin-coated microspheres (MB) (figure 2(A)) was carried out using a modified procedure recommended by Bangs Laboratories [19] using the MCB 1200 biomagnetic processing platform. Briefly, 100 μg of MB were transferred to a 0.5 ml Eppendorf tube. The MB were washed once with 100 μl of TTL buffer and then separated, decanted and resuspended in 20 μl TTL buffer and the desired amount of CF-A (8 μg) added. The resulting solution was incubated for 15 min at a temperature of 25 °C with gentle mixing (400 rpm) in a TS-100 Thermo Shaker. The MB-immobilized CF-A were then separated from the incubation solution and washed sequentially with 100 μl of TT buffer, 100 μl of TTE buffer and 100 μl of TT buffer and then resuspended in 50 μl of the hybridization solution, whereupon it was ready for the first hybridization.

First hybridization procedure. The desired amount of CF-T (1.36 μg; 300 pmol of target) was added to the solution (50 μl) of MB/CF-A conjugate obtained in the previous step (figure 2(B)). The first hybridization reaction was carried out at 25 °C for 15 min in a TS-100 Thermo Shaker (800 rpm) (if not stated otherwise). The MB/CF-A/CF-T conjugate was separated, washed twice with 100 μl of TT buffer, decanted and resuspended in 50 μl of hybridization solution, whereupon it was ready for the second hybridization.

Second hybridization procedure. The desired amount of CF-B (1.36 μg) was added to the solution (50 μl) of MB/CF-A/CF-T conjugate obtained previously (figure 2(C)). This second hybridization reaction was also carried out at 25 °C for 15 min in a TS-100 Thermo Shaker (800 rpm) (if not stated otherwise). The resulting MB/CF-A/CF-T/CF-B conjugate was then washed twice with 100 μl of TT buffer and resuspended in 20 μl of TTL buffer, whereupon it was ready for adding the CdS-QDs–glutathione label.

Binding of CdS-QDs–glutathione. The desired amount of CdS-QDs–glutathione was added to the solution (80 μl) of MB/CF-A/CF-T/CF-B conjugate obtained previously (figure 2(D)). Then the solution was incubated with gentle mixing (400 rpm) for 15 min at 25 °C in a TS-100 Thermo Shaker. The resulting MB/CF-A/CF-T/CF-B/CdS-QDs–glutathione conjugate was washed twice with 100 μl of TT buffer separated, decanted and resuspended in 20 μl of hybridization solution and transferred onto the screen-printed electrode for electrochemical measurements.

2.4. Electrochemical detection

SWV measurements were performed to evaluate the electrochemical behavior of the conjugate CdS QDs. The measurement principle is based on the direct detection of CdS quantum dots using a procedure that was previously developed by our group [20], with the only difference being that the CdS QDs in this case are modified with DNA and linked through hybridization steps with paramagnetic microparticles. The measurements were performed by suspending a volume of 20 μl of the sample (i.e. MB/CF-A/CF-T/CF-B/CdS-QDs–glutathione conjugate suspension) onto the screen-printed electrode (SPE) surface held in the horizontal position covering the three electrodes (W, A and R electrodes) to ensure electrical contact (complete circuit). Each SPE was pretreated, before using, by applying −1.1 V for 300 s as recommended by the SPE supplier [21]. Figure 3 is a schematic of the electrochemical cycle steps applied for each measurement. During the first step (figure 3(A)) a drop of 20 μl CdS QD suspension (CdS QDs DNA conjugate) of known concentration was suspended on the top of the SPE surface. The conjugate was then concentrated onto the working electrode surface using the neodymium magnet (figure 3(B)). During that step a conditioning potential of 0 V was applied for 60 s. The next step (figure 3(C)) was accumulation. In this step a deposition potential of −1.1 V for 120 s was applied to promote the electrochemical reduction of Cd^{2+} ions contained in the CdS QD structure to Cd^0. After the accumulation step, SWV was performed. During this step (figure 3(D)) the potential was scanned from −1.1 to −0.6 V (step potential 10 mV, modulation amplitude 30 mV and frequency 15 Hz): during each an analytical signal due to the oxidation of Cd^0 to Cd^{2+} was obtained. After the SWV measurement the SPE was manually cleaned using the hybridization solution.

The blank subtraction method was performed [22]. The measurement of the blank was performed using the same

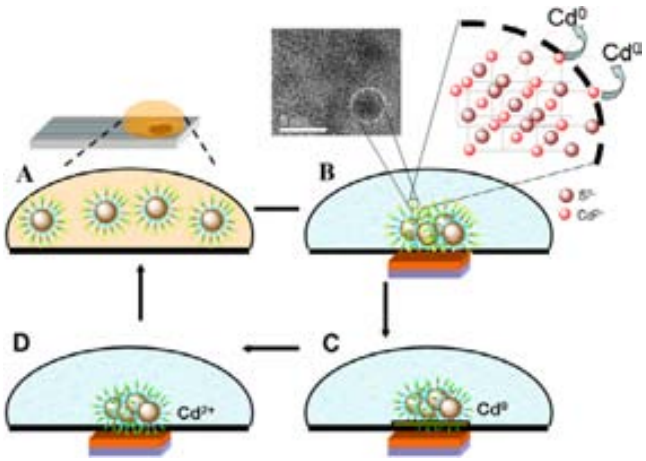

Figure 3. Schematic representation of electrochemical detection of DNA sandwich complex labeled with CdS QDs. (A) Introduction of a drop of 20 μl CdS QD suspension (CdS QDs DNA conjugate) onto the top of the SPE surface. (B) The conjugate is concentrated onto the working electrode surface using the neodymium magnet. A conditioning potential of 0 V was applied for 60 s. (C) A deposition potential of −1.1 V for 120 s was applied during which the cadmium ions are reduced. (D) The reduced cadmium is oxidized back to cadmium ions by SWV scanning from −1.1 to −0.6 V (step potential 10 mV, modulation amplitude 30 mV and frequency 15 Hz).

procedure but using a blank solution (hybridization solution) instead of the CdS QDs DNA conjugate. After this step, using the same sensor, a determined volume of the QD–conjugate suspension is added and measurements (SWV) performed using the 'sample' option. Thus the subtracted curve was obtained for each QD sample.

3. Results and discussion

3.1. Optimizations of the assay parameters

The direct detection of CdS QDs (approximately 3 nm diameter) was previously studied using the same SPEs [20]. The detection method is based on the stripping of electrochemically reduced cadmium at pH 7.0 using square-wave voltammetry. To achieve the analytical signal a deposition potential of −1.1 V for 120 s was applied to promote the electrochemical reduction of Cd^{2+} ions (accessible from the surface of the CdS QDs crystal) (see schematic in figure 3) to Cd^0.

Several parameters regarding the assay procedure have been used on the basis of the previous results or new optimizations performed. The quantity of magnetic particles deposited onto the surface of the SPE is deduced from a previously developed procedure based on the same sandwich DNA using the same magnetic particles but gold nanoparticles instead of quantum dots [12].

The hybridization time (15 min) and temperature (25 °C) used were the same as for the gold nanoparticle assay [12]. For these parameters the assay using 1×10^{21} QDs ml^{-1} shows that, when not using CF-T (blank 1) or CF-B (blank 2), the signals obtained were too high due to the nonspecific adsorptions of QDs onto the surface of the magnetic beads. To avoid this, nonspecific adsorptions of BSA as a blocking agent [23] and lower QD quantities have been checked. BSA is commonly employed as an effective blocking solution in preventing nonspecific binding of non-complementary DNA [24]. It is also used during the preparation of DNA microarrays on a silanized support [25], to block a gold surface [26] or even magnetic beads [27].

The effect of BSA concentration (from 0 to 5%) added after the second hybridization and simultaneously with CdS-QDs–glutathione (1×10^{21} QDs ml^{-1}) upon the SWV peak current was studied by performing the blank assay (the same assay but without CF-B). Figure 1SA (available at stacks.iop.org/Nano/20/055101) shows that the height of the SWV peak decreases by increasing the BSA concentration. This response is related to the improvement of the blocking effect of BSA, causing less nonspecific adsorption of CdS QDs. The minimum current value was obtained when 5% BSA was used for blocking. The effect of the CdS-QDs–glutathione concentration was also studied (figure 1SB (available at stacks.iop.org/Nano/20/055101)) for a fixed concentration of BSA (5%). The increase in the height of the SWV peak by increasing the CdS concentration (from 0.1 to 10×10^{19} QDs ml^{-1}) was observed. The results show that the optimal concentration of CdS-QDs–glutathione obtained is 1.1×10^{19} QDs ml^{-1}.

Figure 2S (available at stacks.iop.org/Nano/20/055101) summarizes the typical responses obtained for the positive assay (A) and the control assays (B, C) studied. Well-shaped SWV curves were obtained when the optimized parameters had been applied while the control assays gave non-significant peaks. Curve A corresponds to the assays with 34 μg ml^{-1} CF-T using DNA probes and other parameters as mentioned before. The oxidation peak of Cd at around −0.72 V, which corresponds to CdS QDs linked to the magnetic particles via DNA hybridization, is shifted by 170 mV toward negative potentials in comparison to CdS QDs (−0.89 V) without DNA and magnetic particles as reported earlier [20]. This is probably related to the easier reduction of the magnetically collected CdS QDs modified with DNA in comparison to the reduction of CdS without DNA and in the absence of a magnetic field. The presence of magnetic particles better induces the stripping of cadmium ions coming from CdS QDs, making it possible for them to be stripped at almost the same potential as that for the case of the free cadmium ion–cadmium ion solutions (−0.71 V). (See supporting information of [20].)

3.2. Hybridizing assay

Figure 4 (left) shows the square-wave voltammograms that demonstrate the efficacy of the genomagnetic assay using CF-T as the target. Three typical calibration curves obtained with three different sensors have been shown. The peak current shows a good linear relationship (figure 4, right) with the concentration of the QD-modified CF-T in the range from 6.8 to 68 μg ml^{-1}, with a correlation coefficient of 0.9998, according to the following equation: $Ip(\mu A) = 0.0087[\text{target}](\mu g\ ml^{-1}) + 0.258$ $(n = 4)$.

The lowest specific signal recorded for the target strand was 6.83 μg ml^{-1} (30 pmol in 20 μl or 1.5 μM). The limit

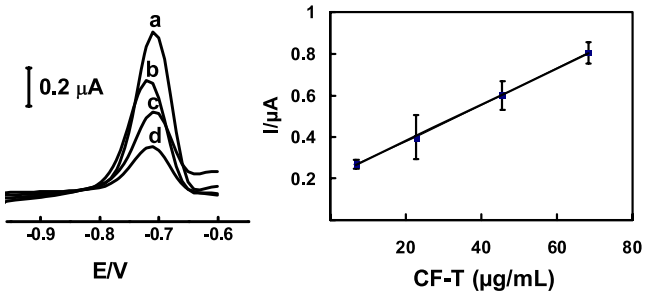

Figure 4. Square-wave stripping voltammograms after blank subtraction to increase concentrations of CF-T: (a) 68, (b) 45, (c) 23 and (d) 6.8 μg ml^{-1}. Also shown is the corresponding calibration plot (right) over the range 6.8–68 μg ml^{-1} of CF-T. The measuring solution was the hybridization solution. Square-wave voltammetric scan with frequency of 25 Hz, step potential 10 mV and amplitude of 30 mV was performed. The deposition potential of −1.1 V for 120 s was applied. Other experimental conditions are as explained in the text.

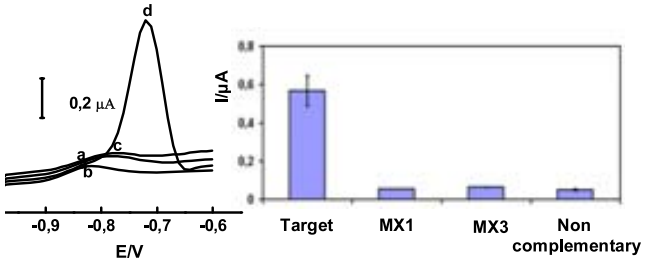

Figure 5. Square-wave stripping voltammograms after blank subtraction for assays performed with: (a) non-complementary sequence, (b) three-mismatch basis, (c) one-mismatch basis and (d) target. The concentrations of each DNA were 7.5 μM. Also shown is the corresponding diagram of the current peak heights (right).

of detection (LOD) is also calculated as 3σ, where σ is the standard deviation obtained for the non-complementary DNA (CF-NC). In our case LOD = 1.82 μg ml^{-1} (for 8 pmol CF-T). The obtained LOD is higher than that obtained by Chang *et al* [28]. Nevertheless the quantum-dot-based technique has the advantage of the possibility for multidetection based on the use of several quantum dots.

The lowest specific signal recorded is almost the same as that obtained using gold nanoparticles (33 pmol in 50 μl) reported earlier by our group [12] but with the advantage of detecting at a lower sample volume (20 μl instead of 50 μl) in connection to a low cost, miniaturized and user-friendly sensor and detection system.

The response of the developed sensor to non-complementary DNA (CF-NC), one (CF-MX1) and three (CF-MX3) mismatch DNA was also checked. Figure 5 shows a well-defined signal for 150 pmol CF-T (around 0.8 μA) along with a good discrimination of CF-NC, CF-MX1 and CF-MX3 (all less than 0.1 μA).

The developed assay provides better discrimination of the DNA mismatches avoiding the use of stringent conditions (i.e. formamide) used for such a purpose [29].

Table 2 shows the measured peak currents and the calculated hybridization efficiencies for four oligonucleotides used in this study: CF-T, CF-NC, CF-MX1 and CF-MX3. These results show that the hybridization efficiency for CF-T is almost 10 times higher than for CF-NC, CF-MX1 and CF-MX3. The efficiencies obtained for the mismatches and the non-complementary DNA are even lower than those reported by Guan *et al* (47 and 60% for TC and TG mismatches, respectively) [28] or almost 50% for the SNP as observed in the study by Cai *et al* (see figure 4 of [30]).

The technology reported here offers various advantages, such as simplicity, sensitivity and effective discrimination against mismatched and non-complementary oligomers. Moreover, using a handheld device and screen-printed electrodes the detection methodology is compatible with the possibility for rapid analysis even in a doctor's surgery with the minimum waste of reagents and low cost.

Table 2. Comparison of hybridization efficiencies of one mismatch (CF-MX1), three mismatches (CF-MX3), non-complementary (CF-NC) and perfect match hybridization (CF-T).

Assays[a]	Peak current (nA)	Hybridization (%)[b]
Perfect match (CF-T)	566	100
3 mismatches (CF-MX3)	64	10
1 mismatch (CF-MX1)	56	11
Non-complementary (CF-NC)	50	9

[a] The concentration of the target oligonucleotide in four hybridizations was 7.5 μM.

[b] The hybridization efficiencies were calculated using the peak currents of the mismatched hybridizations against that of the perfect hybridizations.

4. Conclusions

An electrochemical genomagnetic hybridization assay that takes advantage of an efficient magnetic separation/mixing process and the use of cadmium sulfide nanoparticle tracers for DNA detection has been developed. It combines the magnetic isolation of a DNA hybridization sandwich with the efficient, direct and sensitive electrochemical detection of electroactive nanoparticles. The developed assay employs paramagnetic microparticles modified with streptavidin and linked through a sandwich hybridized DNA target and probes and the use of CdS QDs as electrochemical tags. The detection method is simple and based on the use of screen-printed electrodes as a detection platform and a handheld potentiostatic device as a measuring system. The detection is based on the stripping of electrochemically reduced cadmium at hybridization solution using square-wave voltammetry. The nonspecific signal was eliminated using BSA to block the magnetic bead surface, making it possible to discriminate the target from mismatched and non-complementary DNA strands.

The proposed method allows for the simultaneous detection of quantum-dot-modified DNA in a similar way to that reported earlier [17] but with the difference of direct detection on the surface of the electrode rather than the previous method of dissolving quantum dots. In addition to this, there is a possibility of applying the same detection methodology to an array composed of several electrodes and using the same quantum dot but allowing for the simultaneous

and independent detection of each tag connected with the corresponding DNA target.

Acknowledgment

This work was financially supported by MAT2008-03079/NAN (from MEC, Madrid).

References

[1] Vo-Dinh T, Isola N, Alarie J P, Landis D, Griffin G D and Allison S 1998 *Instrum. Sci. Technol.* **26** 503
[2] Cao Y W, Jin R and Mirkin C A 2002 *Science* **297** 1536
[3] Taton T A, Lu G and Mirkin C A 2001 *J. Am. Chem. Soc.* **123** 5164
[4] Brinkley M 1992 *Bioconjug. Chem.* **3** 2
[5] Takalo H, Mukkala V, Mikola H, Liitti P and Hemmilä I 1994 *Bioconjug. Chem.* **5** 278
[6] Hakala H, Mäki E and Lönnberg H 1998 *Bioconjug. Chem.* **9** 316
[7] Prieto H *et al* 2007 *J. Agricult. Food Chem.* **55** 9208
[8] Pividori M I, Merkoçi A and Alegret S 2003 *Biosens. Bioelectron.* **19** 473
[9] Reed M W, Panyutin I G, Hamlin D, Lucas D D and Wilbur D S 1997 *Bioconjug. Chem.* **8** 238
[10] Kuijpers W H A, Bos E S, Kaspersen F M, Veeneman G H and Van Boeckel C A A 1993 *Bioconjug. Chem.* **4** 94
[11] Wang J, Liu G and Zhu Q 2003 *Anal. Chem.* **75** 6218
[12] Castañeda M T, Merkoçi A, Pumera M and Alegret S 2007 *Biosens. Bioelectron.* **22** 1961
[13] Merkoçi A, Aldavert M, Marín S and Alegret S 2005 *Trends Anal. Chem.* **24** 341
[14] Wang J, Xu D, Kawde A and Polsky R 2001 *Anal. Chem.* **73** 5576
[15] Niu L and Knoll W 2007 *Anal. Chem.* **79** 2695
[16] Merkoçi A, Marín S, Castañeda M T, Pumera M, Ros J and Alegret S 2006 *Nanotechnology* **17** 2553
[17] Wang J, Liu G and Merkoçi A 2003 *J. Am. Chem. Soc.* **125** 3214
[18] Barglik-Chory Ch *et al* 2003 *Chem. Phys. Lett.* **379** 443
[19] Bangs Laboratories Inc. 1999 *Technote 101, ProActive Microspheres* www.bangslabs.com
[20] Merkoçi A, Marcolino-Junior L H, Marín S, Fatibello-Filho O and Alegret S 2007 *Nanotechnology* **18** 035502
[21] Palchetti I, Majid S, Kicela A, Marraza G and Mascini M 2003 *Int. J. Environ. Anal. Chem.* **83** 701
[22] Palchetti I, Laschi S and Mascini M 2005 *Anal. Chim. Acta* **530** 61
[23] Steinitz M 2000 *Anal. Biochem.* **282** 232
[24] Taylor S, Smith S, Windle B and Guiseppi-Elie A 2003 *Nucleic Acids Res.* **31** e87
[25] Lillis B, Manning M, Berney H, Hurley E, Mathewson A and Sheehan M M 2006 *Biosens. Bioelectron.* **21** 1459
[26] Zhi Z, Powell A K and Turnbull J E 2006 *Anal. Chem.* **78** 4786
[27] Morozova T Y and Morozov V N 2008 *Anal. Biochem.* **374** 263
[28] Chang H, Yuan Y, Shi N and Guan Y 2007 *Anal. Chem.* **79** 5111
[29] De la Escosura-Muñiz A, González-García M B and Costa-García A 2007 *Biosens. Bioelectron.* **22** 1048
[30] Cai H, Xu Y, Zhu N, He P and Fang Y 2002 *Analyst* **127** 803

Supporting information

Direct electrochemical stripping detection of cystic fibrosis related DNA linked through cadmium sulphide quantum dots

Sergio Marin, Arben Merkoçi[*]

Nanobioelectronics & Biosensors Group, Institut Català de Nanotecnologia,

&

Department of Chemistry, Universitat Autònoma de Barcelona, Bellaterra, Barcelona, Catalonia, Spain

* ICREA, Barcelona, Catalonia, Spain

[*] Corresponding author: Tel.: +34-93-586-80-14; fax: +34-93-581-23-79; e-mail: arben.merkoci.icn@uab.es

Figure 1S. (A) Optimizations of BSA concentration that was used in the final step of DNA protocol (B) Quantum dots concentration optimization. The experimental conditions are explained in the text.

Figure 2S. Square wave voltammograms of (A) the normal assay (34 μg ml-1of CF-T); (B) The blank does not contain the CF-B (C) blank does not contain the CF-T. The experimental conditions are explained in the text.

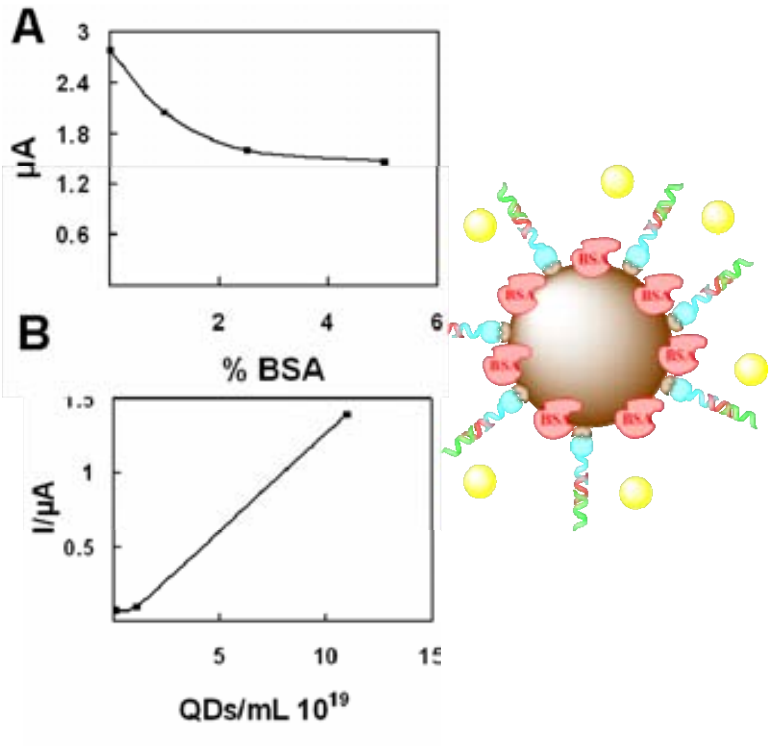

Figure 1S

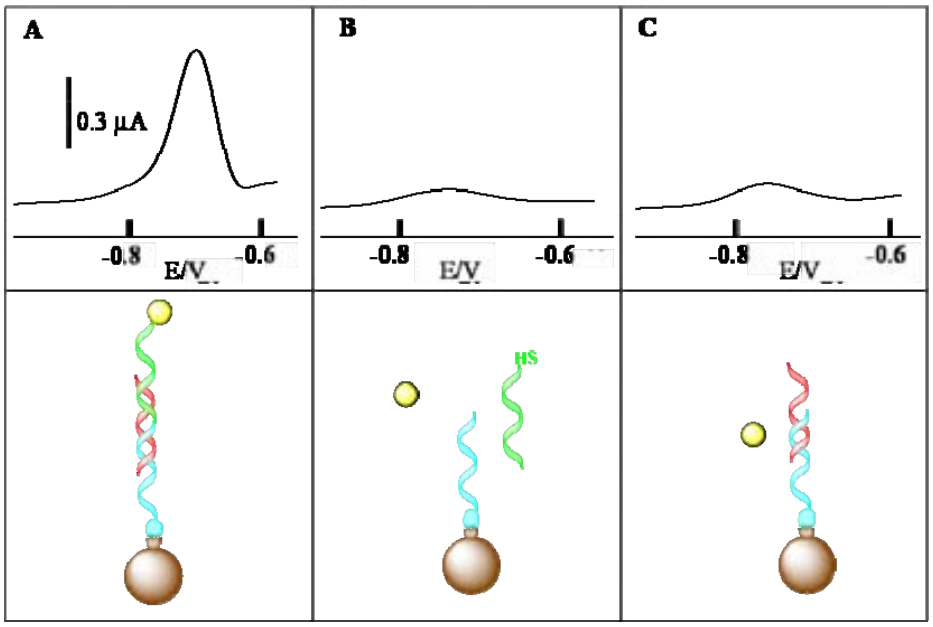

Figure 2S

Chapter 9

Annex

Electrochemical interrogation of cellular uptake of quantum dots decorated with a proline-rich cell penetrating peptide

Marín S., Pujals S., Giralt E., Merkoçi A.

J. Am. Chem. Soc. (communication)

Prepared manuscript sent for publication (2009)

Electrochemical interrogation of cellular uptake of quantum dots decorated with a proline-rich cell penetrating peptide

Sergio Marín[1, 2], Sílvia Pujals[3], Ernest Giralt[3,4,*] and Arben Merkoçi[1,2,5,*]

[1]*Nanobioelectronics & Biosensors Group, CIN2 (ICN-CSIC) Institut Català de Nanotecnologia,*

[2]*Department of Chemistry, Universitat Autònoma de Barcelona, Bellaterra, Barcelona, Catalonia, Spain*

[3]*Institute for Research in Biomedicine, Barcelona, Barcelona Scientific Park*

[4]*Department of Organic Chemistry, University of Barcelona*

[5]*ICREA, Barcelona, Spain*

RECEIVED DATE (automatically inserted by publisher); arben.merkoci.icn@uab.es ; ernest.giralt@irbbarcelona.org

Quantum dots (QDs) are emerging as a new class of fluorescent labels for molecular, cellular, and *in vivo* imaging applications, due to their special optical properties such as a narrow and size-tuneable emission spectra, broad absorption profiles, superior photostability and excellent resistance to chemical degradation or photodegradation with respect to fluorescent dyes.[1] QDs decorated with different types of biomolecule, for example antibodies[2], peptides[3] and DNA[4] able to interact with cells and that provide biological compatibility have been used. The use of QDs and other nanoparticles as tags for electrochemical detection of DNA[5] (including codified technology)[6] and proteins[7] has been extensively studied. An ICPMS-linked DNA assay based on gold nanoparticles immunoconnected through a peptide sequence has also been developed by our group.[8]

Cell-penetrating peptides (CPPs) have been conceived as potential vectors to carry drugs that have low bioavailability across cell membranes.[9]Different CPPs have been described to efficiently deliver various types of cargo to the inside of cells: from low molecular weight drugs to liposomes and plasmids. Among CPPs, the so-called SAP (Sweet Arrow Peptide) combines the ability to translocate the plasma membrane with a virtually complete lack of cytotoxicity.[9,10] SAP shares with other CPPs the presence of positively charged guanidinium groups, a feature that is considered very important for the cellular uptake.[11] In addition, in aqueous medium, SAP adopts a strongly amphipathic helical conformation.[12]

We are particularly interested in electrochemical interrogation of the QDs cellular uptake because (1) previously reported methods based either on imaging techniques or on flow cytometry are both time consuming and usually related to more sophisticated and larger setups; (2) the electrochemical methods are simpler, lower cost and offer additional opportunities in relation to parallel monitoring of several other parameters where the electron transfer can be measured.[13]

Following electrochemical methods the effect of anti-tumor drugs on the growth of immobilized tumor cells was performed by an irreversible voltammetric response related to the oxidation of guanine.[14] Ding et al. immobilized living cells on glassy carbon electrode and the proliferation of cells was measured by an electrochemical impedimetric technique due to the increase in the electron-transfer resistance by the growth of cells.[15]

In the present manuscript we report on the use of square wave voltammetry to monitor the cellular uptake, in HeLa cells, of QDs decorated with SAP.

CdS QDs modified with glutathione have been prepared using the arrested precipitation method as described previously[16] (See Supporting Information for more details). A SAP derivative containing an additional N-terminal cysteine residue (C-SAP) was synthesized using the solid phase method[10] and conjugated to QDs. QDs-SAP conjugation was carried out by mixing C-SAP with CdS QDs (See Supporting Information for more details). Figure S1 shows that the charge of the QDs (-44 mV) was shifted to less negative values (-2mV), a clear indication of the presence of the positively charged guanidinium groups from SAP molecules on the surface of the nanocrystal, a feature that should promote QD cellular uptake.

The interaction of SAP decorated QDs with HeLa cells was first studied using confocal laser scanning microscopy (CLSM). A QD or QD-SAP solution was incubated with HeLa cells and 2 h later the CLSM study was performed with living cells (see figure 1). The results obtained show that the QDs-SAP are partially internalized and partially remain on the cell membrane. On the contrary, the QDs without SAP did not show any kind of interaction with the cell (see CLSM image of Figure 2).

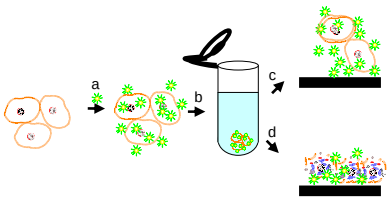

Figure 1. Schematic of the steps followed for CdS QD-SAP interaction with HeLa cells: incubation with QDs (a); separation of the supernatant (b); HeLa cell detection according to the adsorbed QDs (c) and after the cell lysis (d).

The confocal studies of both QDs and QDs-SAP interactions with the cells were followed by electrochemical detection using square wave voltammetry (SWV) as the measuring technique. SWV was previously shown to be a highly sensitive detection technique for CdS QD[17] using Screen Printed Electrodes. Electrochemical measurements of the supernatants after the separation of the HeLa cells (after incubation with QDs or QDs-SAP) have been performed (see supporting information). In addition the electrochemical measurements of either HeLa cell

suspension or lysed HeLa cells (after incubation with QDs or QDs-SAP) have also been carried out.

Figure 2 shows the SWV curve obtained for the living Hela cells incubated with QDs (A, left) and QDs-SAP (B, left). The current magnitude is directly related to the quantity of CdS QDs through the SWV stripping of the corresponding cadmium ions. HeLa cells incubated with QDs non-functionalised with SAP do not interact with the cell membrane, and neither are they internalized, and consequently the SWV did not show a pronounced peak. On the contrary, the current peak of around 2.4 µA is obtained for HeLa cells interacting with CdS QDs-SAP.

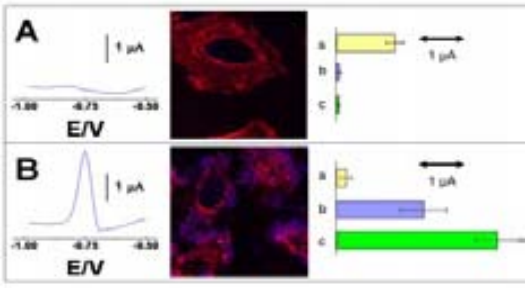

Figure 2. A) SWV of cells incubated with QDs (left); CLSM image (cell-membrane labeled with TRITC-WGA, QD fluorescence signal in blue); SWV peak of the supernatant (a), cells suspension (b) and lysed cells solution (c). B) SWV of cells incubated with QDs-SAP (left); CLSM image (cell-membrane labeled with TRITC-WGA, QD fluorescence signal in blue); SWV peak of the supernatant (a), cell suspension (b) and lysed cells solution (c).

Figure 2 A&B (right bars) show the SWV peaks of supernatant (a), non lysed (b) and lysed (c) HeLa cells. It can be observed that in the case of HeLa cells incubated with QDs non-functionalised with SAP the supernatant contains almost all the CdS QDs used for incubation and consequently the SWV peak is higher (see Figure 2A-a). The SWV of the HeLa cell suspension (obtained after centrifugation and reconstitution with culture medium) did not give a significant peak (Figure 2A-b) which means that there were no QDs attached to the cell surface. The same SWV response was obtained after the HeLa cell lysis, which means no internalization occurred. The same experiments were performed for the case of HeLa cell incubation with SAP's modified QDs. In that case, the QDs concentration in the supernatant was very low (Figure 2B-a) due to the consumption of QDs, either due to cellular uptake (Figure 2B-c) or due to adsorption on the plasma membrane (Figure 2B-b).

The obtained results show that QDs-SAP either interact with the extracellular cell membrane matrix or translocate the bilayer. The first situation, membrane adsorption, is probably a transient state before cellular uptake. Both confocal microscopy and SWV results support the detection of this cellular internalization process. Taking into consideration the electrochemical signals corresponding to the cells (after washing) with the adsorbed QDs-SAP and the lysed solution (released QDs-SAP from the surface and internal uptake) relative percentages of QDs-SAP have been calculated. The QDs-SAP adsorbed onto the cell surface) are a 53 ± 10 % while the internal QDs-SAP represent a 47 ± 10 %.(see details at S3 & S4).

The developed electrochemical detection strategy represents an interesting alternative due to the simplicity of the sensor (screen-printed electrodes) and the measuring instrument (handheld potentiostatic unit).

The obtained results support the continuity of the application of this electrochemical interrogation technique. It can provide valuable insights into the study of peptide-mediated delivery as well as the design and development of nanoparticle probes for intracellular imaging, diagnostic and therapeutic applications. Another important field for future applications could be targeting specific intracellular organelles. Being the nucleus the desirable target because that is where the genetic information on the cell and transcription machinery reside, it could be an increasing research area for such applications. In addition the described electrochemical interrogation is of low cost, is easy to use and offers future interest for diagnostics including cell analysis.

ACKNOWLEDGMENT

This work was supported by MAT2008-03079/NAN (MEC, Madrid); MCI-FEDER (Bio2008-00799, NAN2004-09159-C04-02 and NANOBIOMED-CONSOLIDER) and the Generalitat de Catalunya (CeRBa and 2005SGR-00663). S. Pujals is supported by a FPU grant from the Ministerio de Ciencia e Innovación of Spain. The authors thank Dr. Raquel García Olivas for technical advice on CLSM (UB-SCT).

Supporting Information Available: Apparatus, reagents, synthesis of QDs and SAP, conjugation of QDs-SAP and HeLa cell culture for confocal microscopy and electrochemical measurements.

REFERENCES

(1) (a) Empedocles S., Bawendi M. *Acc. Chem. Res.* **1999**, 32, 389-396. (b) Kuno M., Lee J. K., Dabbosi B. O., Mikulec F. V., Bawendi M. G. *J. Chem. Phys.* **1997**, 106 (23), 9869-9882.(c) Norris D. J., Sacra A., Murray C. B., Bawendi M.G. *Physical Review Letters* **1994**, 72, 2612-2615.

(2) (a) Li-Shishido S., Watanabe T. M., Tada H., Higuchi H., Ohuchi N. *Biochemical and Biophysical Research Communications* **2006**, 351, 7-13. (b) Eggenberger K., Merkulov A., Darbandi M., Nann T., Nick P. *Bioconjugate Chem.* **2007**, 18, 1879-1886. (c) Goldman E.R., Balighian E.D., Mattoussi H., Kumo M. K., Mouro J. M., Tran P. T., Anderson G.P. *J Am. Chem. Soc.* **2002**, 124, 6378-6382.

(3) Silver J., Ou W. Nanoletters 2005, 5, 1445-1449.

(4) (a) Mitchell G. P., Mirkin C. A., Letsinger R. L. J. Am. Chem. Soc. 1999, 121, 8122-8123. (b) Gerion D., Parak W. J., Williams S. C., Zanchet D., Micheel C. M., Alivisatos A. P. J.Am.Chem.Soc. 2002, 124, 7070-7074.

(5) Pumera M., Castañeda M. T., Pividori M. I., Eritja R., Merkoçi A., Alegret A. *Langmuir* **2005**, 21, 9625-9629.

(6) (a) Wang J., Liu G., Merkoçi A., *J. Am. Chem. Soc*. **2003**, 125, 3214-3215. (b) Hansen J. A., Mukhopadhyay R., Hansen J., Gothelf K. V., *J. Am. Chem. Soc.* **2006**, 128, 3860-3861.

(7) (a) Jie G., Huang H., Sun X., Zhu J., *Biosensors and Bioelectronics* **2008**, 23, 1896-1899. (b) Ambrosi, A., Castañeda, M.T., Killard, A.J., Smyth, M.R., Alegret, S., Merkoçi, A. *Analytical Chemistry*, **2007**, 79, 5232-5240

(8) Merkoçi A., Aldavert M., Tarrasón G., Eritja R., Alegret S. *Anal. Chem.* **2005**, 77,6500-6503.

(9) (a) Lundberg P, Langel U, *J. Mol. Recognit.* **2003**, 16(5), 227-33. (b) Futaki S., *Adv. Drug Deliv. Rev.*, **2005**, 57(4), 547-58. (c) Drin G., Cottin S., Blanc E., Rees A. R., Temsamani J. *The Journal of Biological Chemistry* **2003**, 278, 31192-31201. (d) Pujals S., Fernández-Carneado J., López-Iglesias C., Kogan J., Giralt E. *Biochimica et Biophysica Acta* **2006**, 17548, 264-279.

(10) (a) Fernandez-Carneado J., Kogan M. J., Castel S., Giralt E. *Angew. Chem. Int. Edit.* **2004**, 43, 1811-1814. (b) Pujals S., Fernández-Carneado J., Kogan M. J., Martinez J., Cavalier F., Giralt E. *J. Am. Chem. Soc.*, **2006**, 128, 8479-8483.

(11) Pujals, S.; Giralt, E. *Advanced Drug Delivery Reviews* **2008**, 60, 473-484.

(12) Fernández-Carneado, J.; Kogan, M. J.; Pujals, S.; Giralt, E. *Biopolymers (Peptide Science)* **2004**, 76(2), 196-203.

(13) Yang L., Li Y., Erf G. F. *Anal.Chem.* **2004**, 76, 1107-1113.

(14) Du D., Liu S., Chen J., Ju H., Lian H., Li J. *Biomaterials* **2005**, 26, 6487-6495.

(15) Ding L., Hao C., Xue Y., Ju H. *Biomacromolecules* **2007**, 8, 1341-1346.

(16) Merkoçi A., Marín S., Castañeda M. T., Pumera M., Ros J., Alegret S. *Nanotechnology* **2006**, 17, 2553–2559.

(17) Merkoçi A., Marcolino-Junior L. H., Marín S., Fatibello-Filho O., Alegret S. *Nanotechnology* **2007**, 18, 035502 (1-6).

TOC

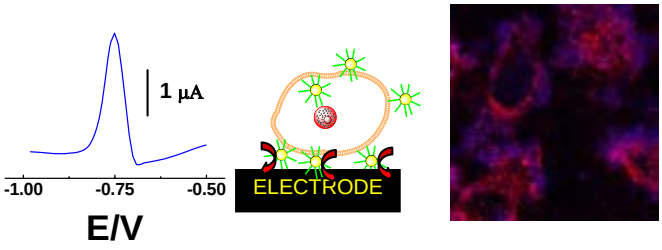

SUPPORTING INFORMATION

Electrochemical interrogation of cellular uptake of quantum dots decorated with a proline-rich cell penetrating peptide

Sergio Marín[1, 2], Silvia Pujals[3], Ernest Giralt[3,4*] and Arben Merkoçi[1, 2,5,*]

[1]*Nanobioelectronics & Biosensors Group, CIN2 (ICN-CSIC) Institut Català de Nanotecnologia,*

[2]*Department of Chemistry, Universitat Autònoma de Barcelona, Bellaterra, Barcelona, Catalonia, Spain*

[3]*Institute for Research in Biomedicine, Barcelona, Barcelona Scientific Park*

[4]*Department of Organic Chemistry, University of Barcelona*

[5]*ICREA, Barcelona, Spain*

Apparatus

Confocal laser scanning microscopy (CLSM) images were obtained using a Leica SPII microscope with a 63X objective.

The ζ–potential measurements were performed using a zetasizer nano zs (Malvern).

All voltammetric experiments were performed using a PalmSens (Palm Instrument BV, Houten, The Netherlands) that consists of a portable potentiostat interfaced with a palmtop PC (155 mm × 85 mm × 35 mm). Electrochemical experiments were carried out using a screen-printed electrode (SPE) (Palm Instrument BV, Houten, The Netherlands). The screen-printed electrochemical cell consists of a graphite working electrode (diameter 3 mm), a graphite counter-electrode and a silver pseudo-reference electrode.

Reagents

Fmoc-Nα-protected amino acids were obtained from IRIS Biotech GmbH (Marktredwitz, Germany). The 2-chlorotrityl chloride resin was purchased from CBL-PATRAS (Patras, Greece). Coupling reagents: 7-azabenzotriazol-1-yloxytris(pyrrolidino)phosphonium hexafluorophosphate, PyAOP, was obtained from Applied Biosystems (Foster City, CA); benzotriazol-1-yloxytris(pyrrolidino)phosphonium hexafluorophosphate, PyBOP, from Novabiochem

(Laüfelfingen, Switzerland); 1-hydroxy-7-azabenzotriazole (HOAt) from GLBiochem (Shanghai, China); and 2-(1Hbenzotriazol-1-yl)-1,1,3,3-tetramethyluronium tetrafluoroborate (TBTU) from Albatros ChemInc. (Montreal, Canada). Trifluoroacetic acid (TFA) was purchased from Scharlab S.L. (Barcelona, Spain). Piperidine, dimethylformamide (DMF), dichloromethane (DCM) and acetonitrile were obtained from SDS (Peypin, France). N,N-diisopropylethylamine (DIEA) was obtained from Merck (Darmstadt, Germany). Triisopropylsilane (TIS) was obtained from Fluka (Buchs, Switzerland).

Synthesis of CdS-QDs. The preparation method is based on arrested precipitation of water dispersed cadmium with sulphide precursors [1]. According to this method 3.228 g glutathione as modifier and 0.799 g $CdCl_2$ were first dissolved in 176 ml water and stirred for 5 min. Subsequently 8.5 ml TMAH (tetramethylammoniumhydroxide) and 315 ml ethanol were added and after 10 min the precursor solution was thoroughly degassed. 0.738 ml HMDST is added quickly to the degassed precursor solution, giving a clear (slightly yellow) colloidal solution of glutathione-coated CdS nanoparticles. The mixture was magnetically stirred for 1 h and the prepared particles were precipitated by adding tetrahydrofuran (THF). One day later the supernatant was decanted and the precipitate was dissolved in water/THF mixture and precipitated again with THF to remove excessive reagents and reaction by-products, respectively. Finally, the supernatant liquid was decanted and the precipitate was dried under vacuum (<1 mbar). The powdery CdS nanoparticles were dissolved again in 0.1 mol l−1 phosphate buffer solution (pH 7.0), obtaining a clear colloidal solution. A stock solution of 1.86×10^{19} CdS QDs ml−1 in milliQ water was prepared and used in further experiments.

Synthesis of SAP. SAP was synthesized on 2-chlorotrityl chloride resin using the 9-fluorenylmethoxycarbonyl/tert-butyl (Fmoc/tBu) strategy and TBTU or PyBOP as coupling reagent. The peptide was cleaved using a cleavage mixture of 95% TFA, 2.5% TIS and 2.5% water. It was purified by semipreparative RP-HPLC, and then characterized by analytical RP-HPLC and MALDI-TOF. For further details, see reference 2.

CdS-QDs modification with SAP. C-SAP was added at a final concentration of 200 μM to a 2.4 mM CdS-QD solution in deionised water, and allowed to react under rapid stirring for 24h at room temperature. Dialysis (M.W.C.O. 6-8000) over deionised water for 3 days was performed to remove peptide excess.

ζ–potential (ZP) measures were made with a Malvern ZetaSizer Nano ZS instrument operating at a light source wavelength of 532 nm and a fixed scattering angle of 173°. These measurements were carried out at pH 7.0, ZP distribution was analysed by intensity.

Cell Culture. HeLa cells were obtained from ATCC (Manasas, VA) and cultured in DMEM (1000 mg/L glucose, Biological Industries) containing 10% fetal calf serum (FCS), 2 mM glutamine, 50 U/mL penicillin, and 0.05 g/mL streptomycin. Exponentially growing HeLa cells were detached from the culture flasks using a trypsin-0.25% EDTA solution, and the cell suspension was seeded at a concentration of 21.4 x 10^3 cells/cm^2 onto glass cover slips, 4-well Lab-Teck chambered coverglass, or plastic dishes (Nalge Nunc International, Rochester, NY).

CLSM cell culture. HeLa cells were incubated with a CdS-QD or CdS-QD-C-SAP solution at 288 μM for 2 h; they were then washed three times with DMEM-10%FCS without phenol red. Then 1 μL of TRITC-WGA was added and confocal laser scanning microscopy was performed using a LeicaSPII microscope with a 63X lens under 364-nm excitation, acquiring 0.25 μm-thick optical sections.

Electrochemical measurements of cell culture. HeLa cells were incubated with a cultured medium containing CdS-QD or CdS-QD-C-SAP solution at 288 μM for 2 h at 37ºC under 5% CO_2. The supernatant was collected separately from the electrochemical measurements and the cells washed afterwards with PBS (3 times with 1.5 mL PBS for 1 min). 200 μL of 0.25 % trypsin-EDTA solution was added to the cells for detachment from the Petri dish followed by 5 min incubation at 37 ºC. Then 1 mL of DMEM was added and the cell suspension was centrifuged (1000 rpm, 4 ºC, 4 min). The supernatant was removed and cells were resuspended in 200 μL of fresh DMEM; 100 μL of this cell suspension were kept in ice for the direct electrochemical measurements. 1 mL of fresh DMEM was added to the remainder and this was again centrifuged (1000 rpm, 4 ºC, 4 min). Supernatant was removed and 100 μL of water was added to the cell pellet and incubated for 1h at 37 ºC for cell lysis.

Electrochemical measurements. The electrochemical measurements were performed suspending a volume of 20 μL over the sensor stripped in the horizontal position, to ensure electrical contact (complete circuit) [3]. Each SPE was pretreated, before use, by applying −1.1 V for 300 s, and then square wave voltammetric (SWV) scans were carried out until a low and stable background was obtained. SWV experiments were

performed to evaluate the electrochemical behavior of the screen-printed electrode (SPE) for CdS QD detection. During this step, a drop of 20 µl containing an appropriate concentration of CdS QDs was suspended onto the SPE for 60 s and a potential of 0 V was applied. The second step was the accumulation step. In this step a deposition potential of −1.1 V for 120 s was applied to promote the electrochemical reduction of Cd^{2+} ions contained in the CdS QD structure to Cd^{0}. After the accumulation step, SWV was performed. During this step the potential was scanned from −1.1 to −0.5 V (step potential 10 mV, modulation amplitude 30 mV and frequency 15 Hz), resulting in an analytical signal due to the oxidation of Cd^{0}. After the SWV measurement the SPE was manually cleaned with a 0.1 mol l−1 phosphate buffer solution (pH 7.0). A blank subtraction method was performed. The blank was measured using a separate blank solution, (0.1 mol l−1) phosphate buffer solution, pH 7.0). After this, using the same sensor, a certain volume of the QD suspension is added and measurements (SWV) performed using the 'sample' option. In this way the subtracted curve was obtained.

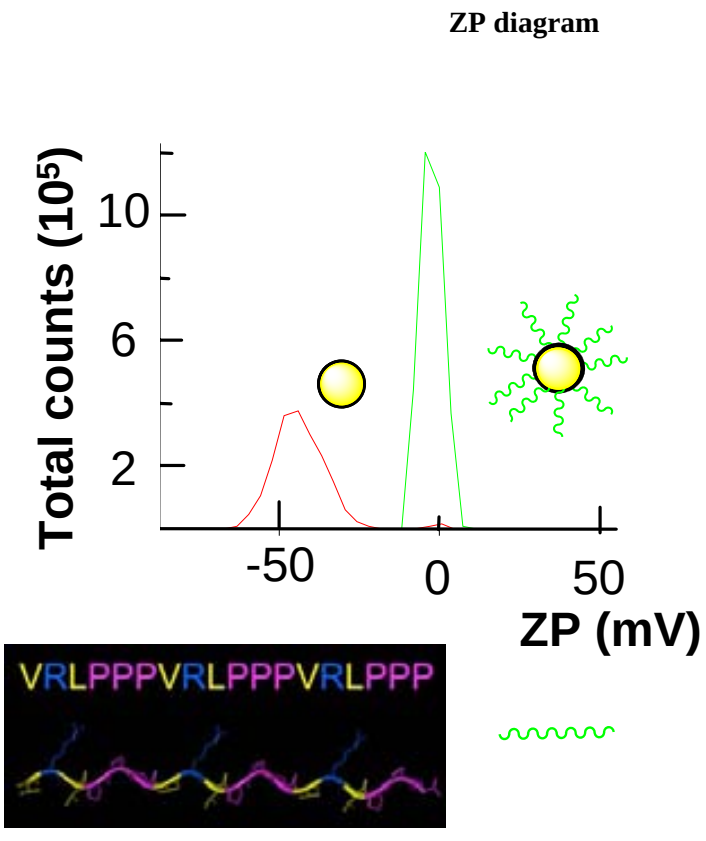

Figure S1. ZP potential diagram of CdS QDs (red) and CdS QDs-SAP (green) (left) and SAP formula and structure, showing a secondary amphipathic structure.

Supplementary CLSM images

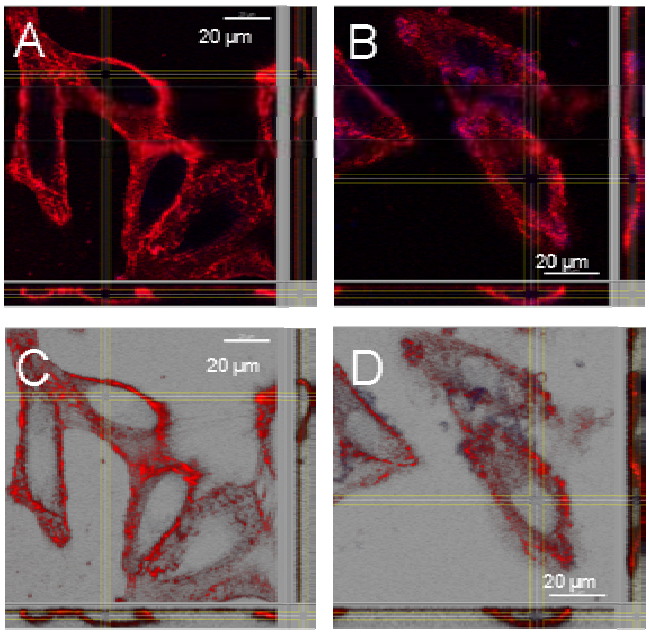

Figure S2. CLSM images of HeLa cells incubated with CdS QD (A, C) and HeLa cells incubated with CdS QD-SAP (B, D). Black contrast (A, B) and white contrast (C, D).

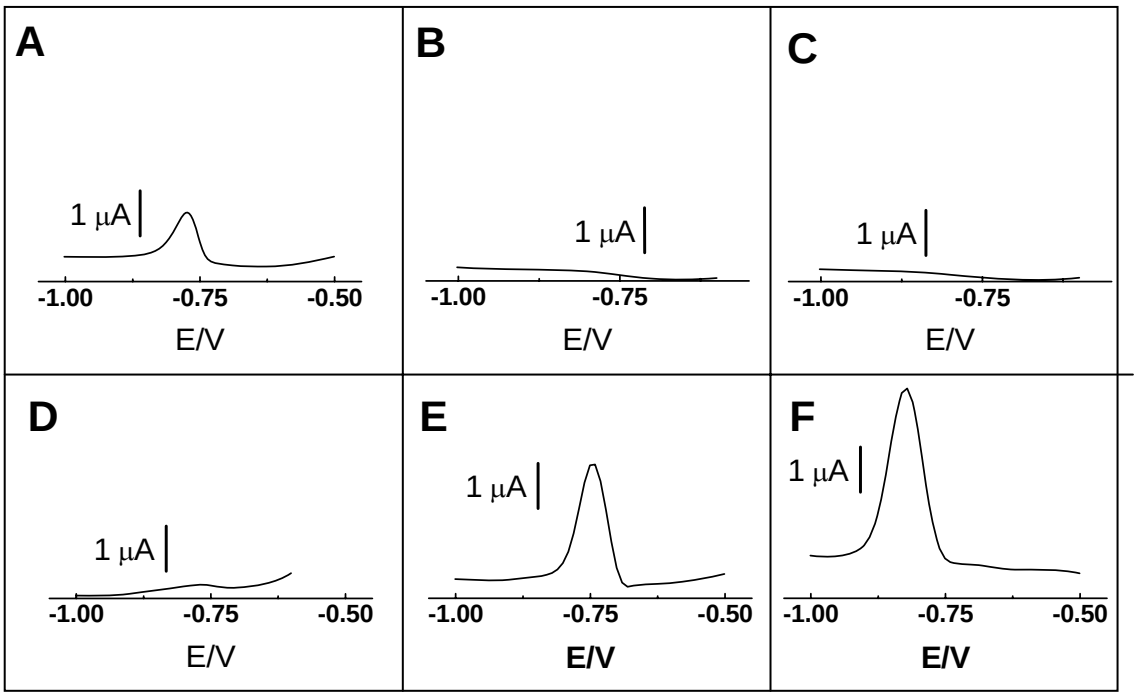

Figure S3. SWV curves of cells incubated with QDs (A,B,C) and with QD-SAP (D,E,F).
A & D correspond to supernatants, B&E to cells and C&F to lysed solution.

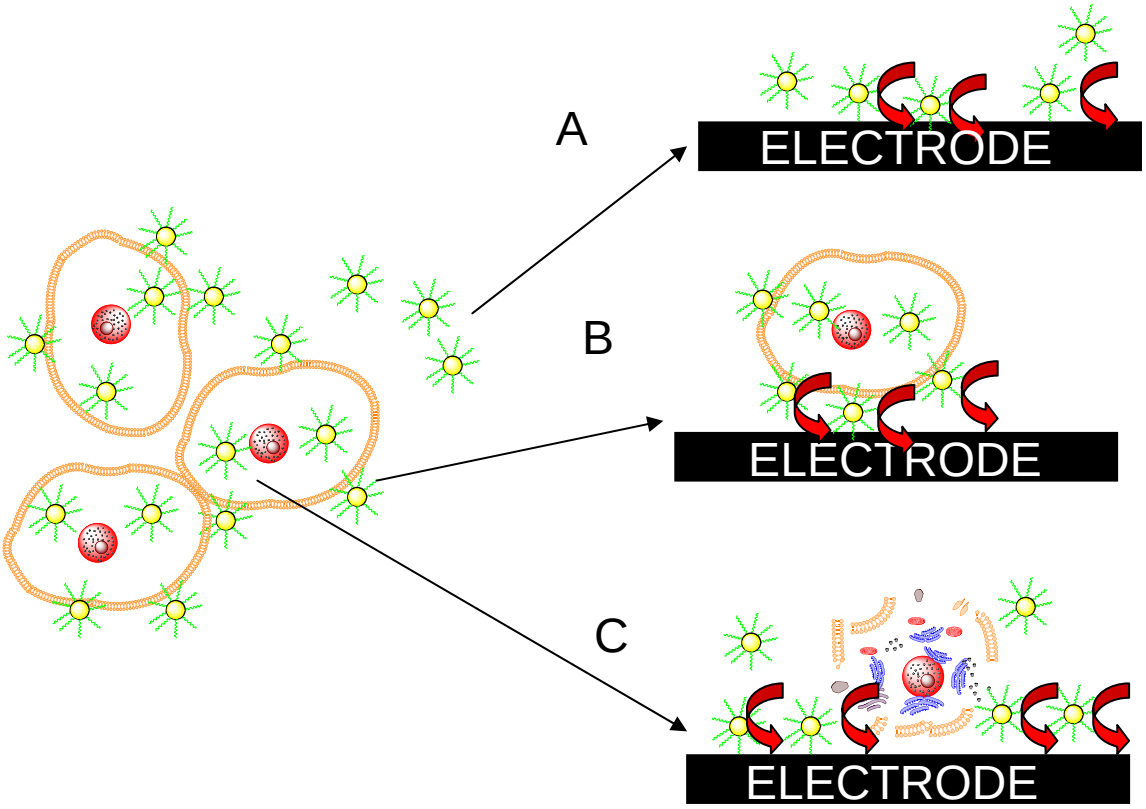

Figure S4.Schemathic representation of the electrochemical detection of cells: (A) Detection of supernatant (the excess / free CdS QDs-SAP is detected); (B) detection of cells with adsorbed QD-SAP; (C) detection of lysed cells (released QDs-SAP that include the adsorbed and the uptake ones).

1) Merkoçi A., Marín S., Castañeda M. T., Pumera M., Ros J., Alegret S. *Nanotechnology* **2006**, 17, 2553–2559.
2) Fernandez-Carneado J., Kogan M. J., Castel S., Giralt E. *Angew. Chem. Int. Edit.* **2004**, 43, 1811-1814.
3) Merkoçi A., Marcolino-Junior L. H., Marín S., Fatibello-Filho O., Alegret S. *Nanotechnology* **2007**, 18, 035502 (1-6).